

NUCLEAR REACTIONS

C.A. BERTULANI

*Department of Physics, Texas A&M University, Commerce, TX 75429, USA**

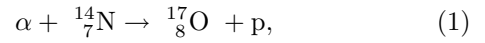
An up-to-date overview of nuclear reactions, from astrophysical to relativistic collision energies. Summary of lecture notes presented at summer schools in Italy and Germany [CB09].

Contents

I. Introduction	1
II. Basic principles	2
A. Conservation laws	2
B. Kinematics	3
C. Cross sections	3
D. Elastic scattering	4
E. Reaction cross sections	4
F. Excitation functions	5
III. Statistical reactions	6
A. Compound nucleus	6
B. Energy spectrum of neutrons	7
C. Resonances	8
D. Statistical theory of nuclear reactions	9
E. The optical model	10
IV. Direct reactions	12
V. Heavy ion reactions	14
A. Types and properties	14
B. Superheavy elements	15
VI. Electromagnetic probes	15
A. Coulomb Excitation	15
B. Photonuclear reactions and giant resonances	16
C. Electron scattering	17
VII. Relativistic nuclear collisions	18
A. Transport theories and equation of state	18
B. Kinematics	19
C. The quark-gluon plasma (QGP)	19
VIII. Nuclear reactions in stars	20
A. Hydrogen and CNO cycles	20
B. Synthesis of heavier elements	22
C. Thermonuclear cross sections	22
IX. Reactions with radioactive nuclear beams	23
Acknowledgments	25
References	25

I. INTRODUCTION

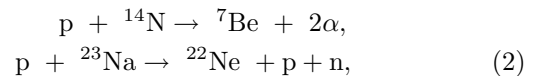
The collision of two nuclei can give place to a nuclear reaction and, similarly to a chemical reaction, the final products can be different from the initial ones. This process happens when a target is bombarded by particles coming from an accelerator or from a radioactive substance. It was in the latter way that Rutherford observed, in 1919, the first nuclear reaction produced in laboratory,



using α -particles from a ${}^{214}\text{Bi}$ sample.

As in eq. 1, other reactions were induced using α -particles, the only projectile available initially. With the development of accelerators around 1930, the possibilities multiplied by changing the energy and mass of the projectile. Today it is possible to bombard a target with protons of energy greater than 1 TeV (1 TeV = 10^{12} eV = 1.602×10^{-7} joules), and beams of particles as heavy as uranium are available for study of reactions with heavy ions.

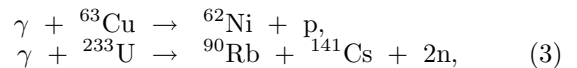
Sometimes we can have more than two final products in a reaction, as in



or just one, as in the capture reaction $\text{p} + {}^{27}\text{Al} \rightarrow {}^{28}\text{Si}^*$, where the asterisk indicates an excited state, which usually decays emitting γ -radiation. Under special circumstances, more than two reactants is possible. Thus, for example, the reaction $\alpha + \alpha + \alpha \rightarrow {}^{12}\text{C}$ can take place in the overheated plasma of stellar interiors.

The initial and final products can also be identical. This case characterizes a process which can be elastic, as $\text{inp} + {}^{16}\text{O} \rightarrow \text{p} + {}^{16}\text{O}$, where there is only transfer of kinetic energy between projectile and target, or inelastic, as in $\text{n} + {}^{16}\text{O} \rightarrow \text{n} + {}^{16}\text{O}^*$, where part of the kinetic energy of the system is used in the excitation of ${}^{16}\text{O}$.

Naturally, nuclear reactions are not limited to nuclei. They could involve any type of particle, and also radiation. Thus, the reactions



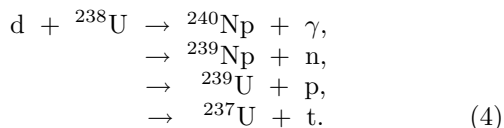
are examples of nuclear processes induced by gamma radiation. In the first case a γ -ray knocks a proton off

arXiv:0908.3275v1 [nucl-th] 22 Aug 2009

*Electronic address: carlos.bertulani@tamu-commerce.edu

^{63}Cu and in the second it induces nuclear fission of ^{233}U , with the production of two fragments and emission of two neutrons.

Unlike a chemical reaction, the resulting products of a nuclear reaction are not determined univocally: starting from two or more reactants there can exist dozens of final products with an unlimited number of available quantum states. As an example, the collision of a deuteron with ^{238}U can give place, among others, to the following reactions:



In the first of them the deuteron is absorbed by the uranium, forming an excited nucleus of ^{240}Np that de-excites by emitting a γ -ray. The two following are examples of *stripping reactions*, in which a nucleon is transferred from the projectile to the target. The last one exemplifies the inverse process: the deuteron captures a neutron from the target and emerges out as ^3H (tritium). This is denoted as a *pick-up reaction*. Another possibility would be, in the first reaction, that ^{240}Np fissions instead of emitting a γ -ray, contributing with dozens of possible final products for the reaction.

Each reaction branch, with well defined quantum states of the participants, is known as *channel*. In 4, for the *entrance channel* $\text{d} + ^{238}\text{U}$, there are four possible *exit channels*. Notice that a different exit channel would be reached if some of the final products were in an excited state. The probability that a nuclear reaction takes place through a certain exit channel depends on the energy of the incident particle and is measured by the *cross section* for that channel.

Nuclear reactions proceed through many possible distinct mechanisms. For instance, in *direct reactions* the projectile and the target have an interaction of short duration, with possible exchange of energy or particles between them. Another mechanism involves the *fusion* of the projectile with the target, the available energy being distributed among all nucleons, forming a highly excited *compound nucleus*. The decay of the compound nucleus leads to the final products of the reaction.

In high energies collisions, the nuclei fragment and particles that were not initially present are produced (for instance, pions, kaons, etc.). The reactions proceed through an intermediate phase in which the nuclear matter is compressed. At very high energies the quarks and gluons inside nucleons become “free” for a short time forming the *quark-gluon plasma*. The study of high energy reactions with nuclei is very important for a better understanding of what happens during spectacular stellar explosions (supernovae) and in the interior of compact stars, as for instance, neutron stars. The study of nuclear reactions at high energies allows to obtain information on the *equation of state* of nuclear matter.

II. BASIC PRINCIPLES

A. Conservation laws

Several conservation laws contribute to restrict the possible processes in a nuclear reaction.

1- *Baryonic number* - There is no experimental evidence of processes in which nucleons are created or destroyed without the creation or destruction of corresponding antinucleons. The application of this principle to low energy reactions is still more restrictive. Below the threshold for the production of mesons (~ 140 MeV), no process related to the nuclear forces is capable to transform a proton into a neutron and vice-versa, and processes governed by the weak force (responsible for the β -emission of nuclei) are very slow in relation to the times involved in nuclear reactions ($\sim 10^{-22}$ to 10^{-16} s). In this way, we can speak separately of proton and neutron conservation, which should show up with same amounts in both sides of a nuclear reaction.

2 - *Charge* - This is a general conservation principle in physics, valid in any circumstance. In purely nuclear reactions it is computed making the sum of the atomic numbers, which should be identical, at both sides of the reaction.

3 - *Energy and linear momentum* - These are two of the most applied principles in the study of the kinematics of reactions. Through them, angles and velocities are related to the initial parameters of the problem.

4 - *Total angular momentum* - is always a constant of motion. In the reaction



^{10}B has $I = 3$ in the ground state, whereas the α -particle has zero angular momentum. If it is captured in an s-wave ($l_i = 0$), the intermediate compound nucleus is in a state with $I_c = 3$. Both final products have intrinsic angular momenta equal to $1/2$. Hence, their sum is 0 or 1. Therefore the relative angular momentum of the final products will be $l_f = 2, 3$ or 4.

5 - *Parity* - is always conserved in reactions governed by the nuclear interaction. In the previous example, ^{10}B , ^4He and the proton have equal parities, while ^{13}C has odd parity. Therefore, if $l_i = 0$, we necessarily have $l_f = 3$. Thus, the orbital momentum of the final products of eq. 5 is determined by the joint conservation of the total angular momentum and of the parity.

6 - *Isospin* - This is an approximate conservation law that is applied to light nuclei, where the effect of the Coulomb force is small. A nuclear reaction involving these nuclei not only conserves the z -component of the isospin (a consequence of charge and baryonic number conservation) but also the total isospin \mathbf{T} . Reactions that populate excited states not conserving the value of \mathbf{T} are strongly inhibited. An example is the reaction $\text{d} + ^{16}\text{O} \rightarrow \alpha + ^{14}\text{N}$, where the excited state 0^+ , with 2.31 MeV, of ^{14}N is about a hundred times more populated than

the 1^+ ground state. Conservation of energy, angular momentum and parity do not impose any prohibition for that channel, whose low occurrence can only be justified by isospin conservation: the ground states of the four participant nuclei in the reaction have all $\mathbf{T} = 0$ and the state 1^+ of ^{14}N has $\mathbf{T} = 1$.

B. Kinematics

We consider a typical reaction, in which the projectile a and the target A gives place to two products, b and B . This can also be expressed in the notation that we used so far, $a + A \rightarrow b + B$, or even in a more compact notation, $A(a,b)B$.

Often, a and b are light nuclei and A and B , heavy ones; the nucleus b being emitted at an angle θ and its energy registered in the laboratory system. The recoiling nucleus B has usually a short range and cannot leave the target. It is convenient to introduce the Q -value of the reaction which measures the energy gained (or lost) due to the difference between the initial and final masses:

$$Q = (m_a + m_A - m_b - m_B)c^2. \quad (6)$$

Using energy and momentum conservation in the reaction, one gets:

$$Q = E_b \left(1 + \frac{m_b}{m_B}\right) - E_a \left(1 - \frac{m_a}{m_B}\right) - \frac{2}{m_B} \sqrt{m_a m_b E_a E_b} \cos \theta. \quad (7)$$

From this relation one obtains that, when Q is negative, an energy threshold exists for the incident particle, E_t , as a function of the angle θ , below which nuclei b are not observed in that angle:

$$E_t = \frac{-Q m_B (m_B + m_b)}{m_a m_b \cos^2 \theta + (m_B + m_b)(m_B - m_a)}. \quad (8)$$

This example shows the power of conservation laws in the analysis of nuclear reactions. Similar to this example, very useful relations can be derived in the relativistic regime, and/or using other conserved quantities.

C. Cross sections

Figure 1 shows schematically a typical scattering experiment. In fact this is the sketch of E. Rutherford experiment in 1910 [2]. Projectiles (here, α -particles) from a source pass through a collimator and collide with a target (gold foil). Some projectiles are scattered by the target and reach the detector (here, a fluorescent screen). Rutherford expected them to go straight through the target, with perhaps minor deflections. Most did go straight through, but to his surprise some particles bounced straight back! Rutherford hypothesized that the

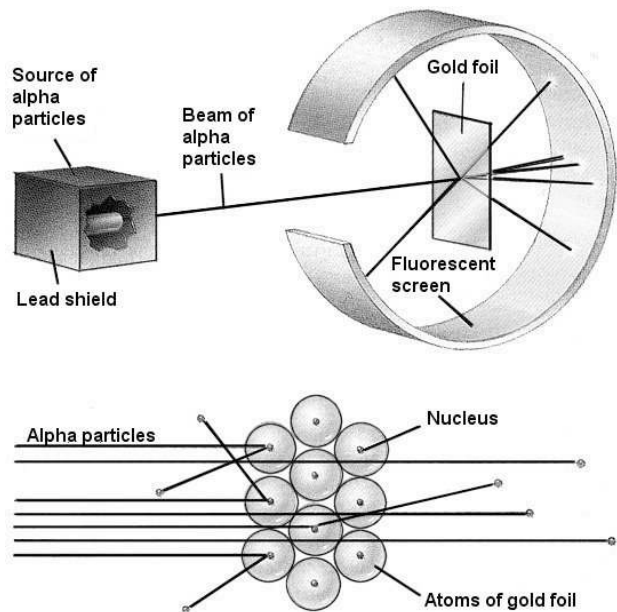


FIG. 1: (Top) Rutherford's scattering experiment with α -particles scattering on a gold foil. (Bottom) Microscopic interpretation of the experimental results.

positive alpha particles had hit a heavy mass of positive particles, which he called *the nucleus*.

Let us consider an experiment as that represented in figure 2, measuring the count rate of events leading to the population of channel- α , $N_\alpha(\Omega, \Delta\Omega)$. Assuming that interactions between beam particles can be neglected, the count rate $N_\alpha(\Omega, \Delta\Omega)$ should be proportional to the incident flux J , to the fraction of solid angle $\Delta\Omega$ where the particles are scattered to, and to the number of target particles per unit volume. Hence, $N_\alpha(\Omega, \Delta\Omega)$ can then be written as $N_\alpha(\Omega, \Delta\Omega) = (\Delta\Omega \cdot n \cdot J) d\sigma_\alpha(\Omega)/d\Omega$. The constant of proportionality,

$$\frac{d\sigma_\alpha(\Omega)}{d\Omega} = \frac{N_\alpha(\Omega, \Delta\Omega)}{\Delta\Omega \cdot n \cdot J}, \quad (9)$$

is called the *differential cross section* for channel- α . This quantity is very useful, since it does not depend on experimental details (detector size, incident flux, target thickness). It depends exclusively on the physics of the projectile and target particles.

Frequently, one is interested in the angle integrated *total cross section* given by

$$\sigma_\alpha = \int d\Omega \left[\frac{d\sigma_\alpha(\Omega)}{d\Omega} \right]. \quad (10)$$

In nuclear physics cross sections are usually measured in units of *barns*. 1 barn corresponds to an area of a circle of diameter approximately equal to $8 \text{ fm} = 8 \times 10^{-15} \text{ m}$. For the comparison between theory and experiment, it is necessary to have cross sections in the same reference frame. Of course, the measured cross section is obtained

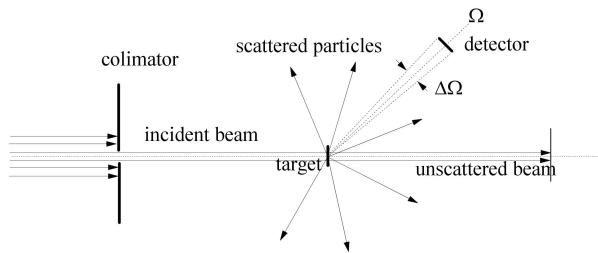


FIG. 2: Schematic representation of a scattering experiment.

in the laboratory frame, where the target is at rest. From the theoretical point of view, however, it is important to take advantage of the translational invariance of the projectile-target Hamiltonian, introducing the center of mass frame (CM). The transformation is done using the laws of conservation of energy and momentum.

The Rutherford experiment has a simple classical description in which one assumes that the α -particles follow hyperbolic trajectories in the Coulomb field of the heavy target. The scattering at an angle θ can be easily calculated and with that one is able to calculate the Coulomb, or Rutherford cross section. The result is

$$\frac{d\sigma_R}{d\Omega} = \left(\frac{Z_P Z_T e^2}{4E} \right)^2 \text{cosec}^4 \left(\frac{\theta}{2} \right), \quad (11)$$

where Z_P (Z_T) is the projectile (target) charge number and E is the CM energy.

D. Elastic scattering

When a beam of particles, represented in quantum mechanics by a plane wave, hits a nucleus the wave function is modified by the presence of a scattering potential $V(r)$, responsible for the appearance of a phase in the outgoing part of the wave. Elastic scattering is just one of the channels for the which the reaction can proceed and is known as *elastic channel*. Inelastic scattering and all the other channels are grouped in the *reaction channel*.

The occurrence of a nuclear reaction through a given reaction channel leads to a modification of the outgoing part of the wave function not only by a phase factor, but also by changing its magnitude, indicating that there is a loss of particles in the elastic channel. For a projectile with momentum $p = \hbar k$, this can be expressed by

$$\Psi \sim \frac{1}{2i} \sum_{l=0}^{\infty} (2l+1) i^l P_l(\cos\theta) \frac{\eta_l e^{i(kr-l\pi/2)} - e^{-i(kr-l\pi/2)}}{kr}, \quad (12)$$

where the complex coefficient η_l is the factor mentioned above. If $\eta = 1$, the sum in eq. 12 can be done analytically, leading to $\Psi \sim \exp(i\mathbf{k}\cdot\mathbf{r})$, i.e. a plane wave. But if $\eta_l = \exp[i\delta_l]$, with δ_l real, the incoming and outgoing

waves have the same magnitude, i.e. the scattering is elastic.

The sum in eq. 12 is known as *partial wave expansion* of the scattering wave. The label $l = 0, 1, 2, \dots = (s, p, d, \dots \text{ waves})$ denotes the contribution of a particular angular momentum (in units of \hbar) to the total wavefunction. Classically the angular momentum of an incident particle is given by $l = kR$, where R is known as *impact parameter* which is the perpendicular distance to the target if the projectile were undeflected. In quantum mechanics l is not continuous, varying in steps of one.

We can rewrite eq. 12 as a sum of a plane wave and a scattering outgoing wave in the form $\Psi \sim \exp(i\mathbf{k}\cdot\mathbf{r}) + f(\theta)e^{ikr}/r$, where $f(\theta)$ accounts for the distortion of the outgoing wave at the scattering angle θ . It is known as the *scattering amplitude*:

$$f(\theta) = \frac{1}{2ik} \sum_{l=0}^{\infty} (2l+1)(\eta_l - 1)P_l(\cos\theta). \quad (13)$$

One can now calculate the cross section by counting the number of particles that are scattered through angle θ . This can be done by calculating the particle current associated with the wavefunction Ψ . One gets the differential scattering cross section

$$\frac{d\sigma_e}{d\Omega} = |f(\theta)|^2 = \frac{1}{4k^2} \left| \sum_{l=0}^{\infty} (2l+1)(1 - \eta_l)P_l(\cos\theta) \right|^2. \quad (14)$$

The total scattering cross section, eq. 10 becomes

$$\sigma_e = \pi \bar{\lambda}^2 \sum_{l=0}^{\infty} (2l+1) |1 - \eta_l|^2, \quad (15)$$

with $\bar{\lambda} = \lambda/2\pi = 1/k$.

E. Reaction cross sections

To calculate the reaction cross section it is necessary to compute the number of particles that disappear from the elastic channel, what is measured by the flux of the current of probability vector through a spherical surface of large radius centered at the target, calculated with the total wave function of eq. 12. One finds

$$\sigma_r = \pi \bar{\lambda}^2 \sum_{l=0}^{\infty} (2l+1)(1 - |\eta_l|^2). \quad (16)$$

From equations 15 and 16: when $|\eta_l| = 1$ the reaction cross section is zero and we have pure scattering. The contrary, however, cannot happen, as the vanishing of σ_e also implies in the vanishing of σ_r . In general there is a region of allowed values of η_l for which the two cross sections can coexist.

The maximum of σ_r happens for $\eta_l = 0$, what corresponds to total absorption. Let us suppose that the

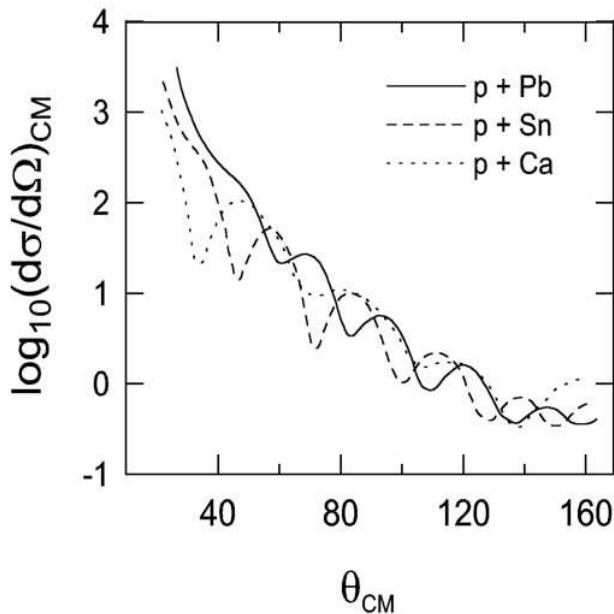


FIG. 3: Elastic scattering angular distribution of protons of 30 MeV on Ca, Sn and Pb. The curves are adjusted to the experimental data of ref. [3]

absorption potential is limited to the surface of a nucleus with radius $R \gg \bar{\lambda}$, that is, that all the particles with impact parameter smaller than the radius R are absorbed. That is equivalent to say that all particles are absorbed for $l \leq R/\bar{\lambda}$. In this case

$$\sigma_r = \pi \bar{\lambda}^2 \sum_{l=0}^{R/\bar{\lambda}} (2l+1) = \pi (R + \bar{\lambda})^2. \quad (17)$$

This is the value that would be intuitively adequate for the total cross section, i.e., equal to the geometric cross section (the part $\bar{\lambda}$ can be understood as an uncertainty in the position of the incident particle). But, we saw above that the presence of scattering is always obligatory. For $\eta_l = 0$, the scattering and reaction cross sections are identical, yielding the total cross section

$$\sigma = \sigma_r + \sigma_e = \pi (R + \bar{\lambda})^2 + \pi (R + \bar{\lambda})^2 = 2\pi (R + \bar{\lambda})^2 \quad (18)$$

that is twice the geometric cross section!

The presence of the scattering part, that turns the result 18 apparently strange, can be interpreted as the effect of diffraction of the plane waves at the nuclear surface. This effect leads to “shadow” behind the nucleus decreasing its apparent diameter so that, at a certain distance, the perturbation caused by the presence of the nucleus disappears and the plane wave is reconstructed. In this situation we can say that the part of the beam which is diffracted has to be the same as the part that is absorbed, justifying the equality of σ_r and σ_e . The diffraction phenomenon appears clearly in the elastic scattering or inelastic angular distribution (differential cross section

as function of the scattering angle): figure 3 exhibits angular distributions for the elastic scattering of 30 MeV protons on ^{40}Ca , ^{120}Sn and ^{208}Pb . The oscillations in the cross sections are characteristic of a *Fraunhofer diffraction* figure, similar to light scattering by an opaque disk. The angular distance $\Delta\theta$ between the diffraction minima follows closely the expression $\Delta\theta = \hbar/pR$, characteristic of diffraction phenomena.

F. Excitation functions

When the projectile has a very low energy, $k \rightarrow 0$, and in particular, $l = kR \ll 1$. As an example consider the scattering of neutrons with $l = 0$ and ignore the spins of the neutron and of the target. In this case the *Schrödinger equation* for the radial motion of the neutron with respect to the target is

$$\frac{d^2 u_0}{dr^2} + k^2 u_0 = 0 \quad (r \geq R). \quad (19)$$

This is valid for the radial wave function u_0 at distances r larger than the *channel radius* $R = R_a + R_A$, with R_a and R_A being the radii of the projectile and of the target, respectively. The solution of eq. 19 is

$$u_0 = \eta_0 e^{ikr} - e^{-ikr} \quad (r \geq R). \quad (20)$$

A radial wave function inside the nucleus should connect to the external function 20 with a continuous function and its derivative at $r = R$. That is, the function

$$f_l \equiv R \left[\frac{du_l/dr}{u_l} \right]_{r=R} \quad (21)$$

must have identical values if calculated with the internal or the external function and this condition creates a relationship between f_l and η_l . Hence, the knowledge of f_l leads to the knowledge of the cross sections. For neutrons with $l = 0$, the application of 20 results in

$$f_0 = ikR \frac{\eta_0 + e^{-2ikR}}{\eta_0 - e^{-2ikR}}, \quad (22)$$

from which we extract

$$\eta_0 = \frac{f_0 + ikR}{f_0 - ikR} e^{-2ikR}. \quad (23)$$

If f_0 is a real number, then $|\eta_0|^2 = 1$. The reaction cross section, eq. 16, will be zero and we have pure scattering.

Using eq. 23, the scattering cross section, eq. 15, can be written as

$$\sigma_{e,0} = \pi \bar{\lambda}^2 |A_{res} + A_{pot}|^2, \quad (24)$$

with $A_{res} = \frac{-2ikR}{f_0 - ikR}$ and $A_{pot} = \exp(2ikR) - 1$. The separation of the cross section in two parts has physical justification: A_{pot} does not contain f_0 and therefore does not

depend on conditions inside the nucleus. It represents the situation where the projectile does not penetrate the nucleus as in the idealized situation where the nucleus is considered an impenetrable hard sphere. The wave function is zero inside the nucleus and u_0 vanishes at $r = R$, implying $f_0 \rightarrow \infty$ and $A_{res} \rightarrow 0$. Hence, A_{pot} is the only responsible for the scattering.

Inserting eq. 23 in 16 and using

$$f_0 = f_R + if_I \quad (25)$$

we have

$$\sigma_{r,0} = \pi \bar{\lambda}^2 \frac{-4kRf_I}{f_R^2 + (f_I - kR)^2} \quad (26)$$

an equation that is useful when we study the presence of resonances in the *excitation function* (cross section as a function of the energy).

III. STATISTICAL REACTIONS

A. Compound nucleus

When a low energy neutron (< 50 MeV) enters the range of nuclear forces it can be scattered or begin a series of collisions with the nucleons. The products of these collisions, including the incident particle, will continue in their course, leading to new collisions and new changes of energy. During this process one or more particles can be emitted and they form with the residual nucleus the products of a reaction that is known as *pre-equilibrium*. At low energies, the largest probability is the continuation of the process so that the initial energy is distributed among all nucleons, with no emitted particle. The final nucleus with $A + 1$ nucleons has an excitation energy equal to the kinetic energy of the incident neutron plus the binding energy the neutron has in the new, highly unstable, nucleus [4]. It can, among other processes, emit a neutron with the same or smaller energy to the one absorbed. The de-excitation process is not necessarily immediate and the excited nucleus can live a relatively long time. We say that there is, in this situation, the formation of a *compound nucleus* as intermediary stage of the reaction. In the final stage the compound nucleus can evaporate one or more particles, fission, etc. In our notation, for the most common situation in which two final products are formed (the evaporated particle plus the residual nucleus or two fission fragments, etc.) we write:



the asterisk indicating that the compound nucleus C is in an excited state.

The compound nucleus lives long enough to “forget” how it was formed and the de-excitation to the final products b and B only depends on the energy, angular momentum and parity of the quantum state of the compound

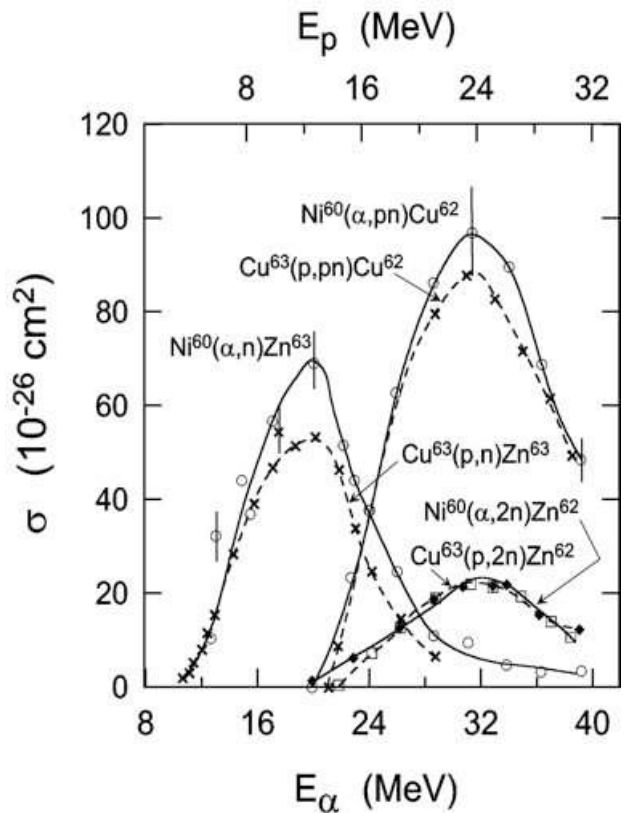
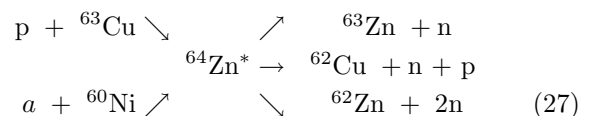


FIG. 4: Cross sections for the reactions shown in 27. The scales of the upper axis (energy of the protons) and lower axis (energy of the α -particle) were adjusted to correspond to the same excitation energy of the compound nucleus [5].

nucleus. An interesting experimental verification was accomplished by S. N. Ghoshal in 1950 [5]. He studied two reactions that take to the same compound nucleus, $^{64}\text{Zn}^*$, and measured the cross sections of three different forms of decay, as shown below:



If the idea of the compound nucleus is valid and if one chooses the energy of the proton and of the incident α -particle to produce the same excitation energy, then the cross section for each one of the three exit channels should be independent of the way the compound nucleus is formed. That is, the properties of the compound nucleus do not have any relationship with the nuclei that formed it. This is confirmed in figure 4, where one sees clearly that the cross sections depend practically only on the exit channels.

The angular distribution of fragments, or evaporated particles, of a compound nucleus should be isotropic in the center of mass, and this is verified experimentally.

However, the total angular momentum is conserved and cannot be “forgotten”. Reactions with large transfer of angular momentum, as when heavy ions are used as projectiles, can show a non-isotropic angular distribution in the center of mass system.

The occurrence of a nuclear reaction in two stages allows the cross section for a reaction $A(a,b)B$ to be written as the product, $\sigma(a,b) = \sigma_c(a,A)P(b)$, where $\sigma_c(a,A)$ is the cross section of formation of the compound nucleus starting from the projectile a and the target A and $P(b)$ is the probability that the compound nucleus emits a particle b leaving a residual nucleus B . If the quantum numbers of entrance and exit channels are well specified, i.e., if the reaction begins at an entrance channel α and ends at an exit channel β , one can write

$$\sigma(\alpha, \beta) = \sigma_c(\alpha)P(\beta). \quad (28)$$

We can associate the probability $P(\beta)$ to the width Γ_β of the channel β and write:

$$P(\beta) = \frac{\Gamma(\beta)}{\Gamma}, \quad (29)$$

where Γ is the total width, that is, $\tau = \hbar/\Gamma$ is the half-life of disintegration of the compound nucleus. Eq. 29 just expresses the fact that the decay probability through channel β is the decay rate through that channel divided by the total decay rate. In the competition between the several channels β , the nucleons have clear preference over the γ -radiation whenever there is available energy for their emission and among the nucleons the neutrons have preference as they do not have the Coulomb barrier as an obstacle. Thus, in a reaction where there is no restriction for neutron emission we can say that

$$\Gamma \cong \Gamma_n, \quad (30)$$

where Γ_n includes the width for the emission of one or more neutrons.

The study of the function $P(\beta)$ is done in an evaporation model that leads to results in many aspects similar to the evaporation of molecules of a liquid, with the energy of the emitted neutrons having the form of a Maxwell-Boltzmann distribution

$$I(E) \propto E \exp\left(-\frac{E}{\theta}\right) dE, \quad (31)$$

with I measuring the amount of neutrons emitted with energy between E and $E + dE$. The quantity θ , with dimension of energy, has the role of a *nuclear temperature*. It is related to the density of levels ω of the daughter nucleus B by

$$\frac{1}{\theta} = \frac{dS}{dE}, \quad (32)$$

with

$$S = \ln \omega(E) \quad (33)$$

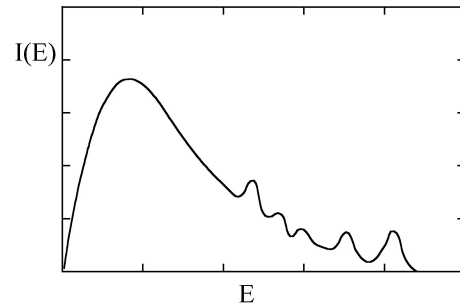


FIG. 5: Energy spectrum of neutrons evaporated by a compound nucleus.

where dS/dE is calculated for the daughter nucleus B at the maximum excitation energy that it can have after the emission of a neutron. That is, in the limit of emission of a neutron with zero kinetic energy.

The level density $\omega(E)$ is a measure of the number of available energy states for the decay of the compound nucleus in the interval dE around the energy E . In this sense, the relationship 33 is, neglecting the absence of the Boltzmann constant, identical to the thermodynamic relationship between the entropy S and the number of states available for the transformation of a system. Eq. 32 is the well-known relation between the entropy and the temperature.

A simple expression for the energy dependence of the state density is provided by the equidistant spacing model which assumes that the one-particle states are equally spaced with spacing d , and that the total energy of the nucleus is simply obtained by adding the energies of the constituent nucleons. The solution of this problem can be obtained from statistical mechanics [10]:

$$\rho(E) \sim \exp\left(2\sqrt{aE}\right).$$

Extensive analyzes of experimental data show that for nuclei far from the region of the magic nuclei a varies linearly with A (or with N and Z), as shown in fig. 6:

$$a \cong \frac{A}{k} \text{ MeV}^{-1}. \quad (34)$$

It is found that $k \cong 7.5 - 8$.

B. Energy spectrum of neutrons

The energy distribution of neutrons emitted by a compound nucleus has the aspect of the curve shown in figure 5. Only the low energy part obeys 31 and the reason is simple: the emission of a low energy neutron leaves the residual nucleus with a large excitation energy, and the level density is very high. The large density of final states turns the problem tractable with the statistical model that leads to 31. In the opposite situation are the low energy states of the residual nucleus. These isolated states

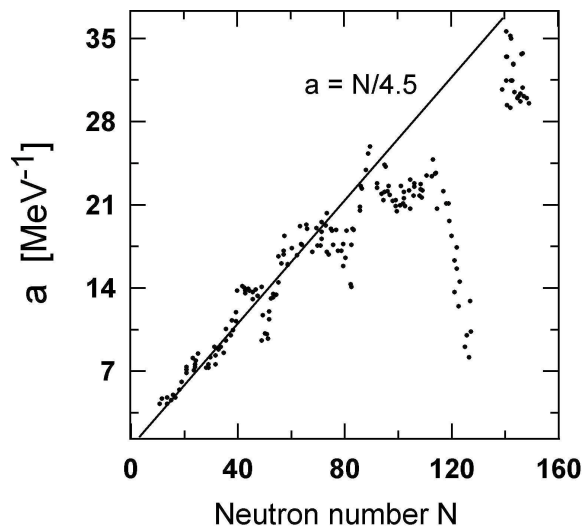


FIG. 6: Values of the level density parameter a as a function of the neutron number. Far from magic regions, $a \approx N/4.5 \text{ MeV}^{-1}$ which approximately corresponds to $a = A/7.5 \text{ MeV}^{-1}$ [13].

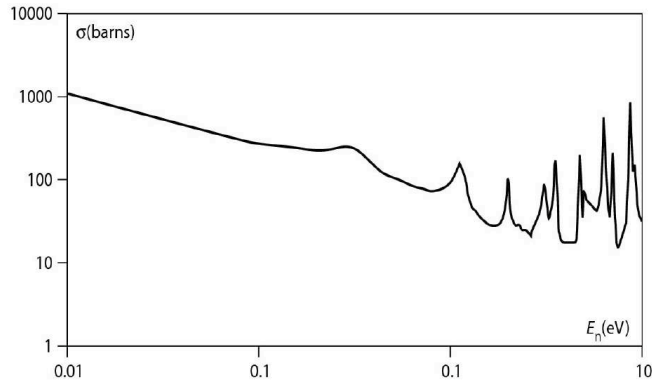


FIG. 7: Total cross section for low energy neutrons hitting ^{235}U .

appear as peaks in the tail of the distribution. When the emission is of a proton or of another charged particle, the form of figure 31 is distorted, the part of low energy of the spectrum being suppressed partially by the Coulomb barrier.

Let us now assume that there is only elastic scattering or formation of compound nucleus. We further assume that the elastic scattering is purely potential, without resonant elastic scattering. That is, there is no re-emission of neutrons with energy equal to the incident projectile. This is equivalent to say that the probability that the exit channel is the same as the entrance channel is very low. According to these assumptions, the cross section $\sigma_c(\alpha)$ of eq. 28 is the reaction cross section of eq. 16. We can still write the wave function inside the nucleus

as just an incoming wave

$$u_0 \cong \exp(-iKr) \quad (r < R), \quad (35)$$

where $K = \sqrt{2m(E - V_0)}/\hbar$ is the wavenumber inside the nucleus, and it is assumed that the neutron with total energy E is subject to a negative potential V_0 . Eq. 35 is clearly a crude simplification when the incident neutron interacts in a complicated way with the other nucleons in the nucleus. It allows, however, to explain the average behavior of the cross sections for low energies. Starting with eqs. 21 and 35 one determines the value of f_0 :

$$f_0 = -iKR \quad (36)$$

and from eq. 26, we get

$$\sigma_c = \pi \bar{\lambda}^2 \frac{4kK}{(k + K)^2} \quad (37)$$

for the cross section of compound nucleus formation for neutrons with $l = 0$. At low energies, $E \ll |V_0|$, thus $k \ll K$. Under these conditions, $\sigma_c = 4\pi/kK$, since $\bar{\lambda} = k^{-1} \gg R$. Thus, σ_c varies with $1/k$. That is,

$$\sigma_c \propto \frac{1}{v}, \quad (38)$$

where v is the velocity of the incident neutron. This is the well-known $1/v$ law that governs the behavior of the capture cross section of low energy neutrons. Figure 7 exhibits the excitation function (cross section as function of the energy) for the reaction $n + ^{235}\text{U}$. The cross section decays with $1/v$ up to 0.3 eV, where a series of resonances appear.

C. Resonances

To understand why there are resonances, we shall use again the simple model of a single particle subject to a square-well potential. We know that inside the well the Schrödinger equation only admits solution for a discrete group of values of energy, E_1, E_2, \dots, E_n . A particle is confined to the interior of the well by reflections that it has at the surface of the well. In these reflections the wave that represents the particle should be in phase before and after the reflection and this only happens for a finite group of energies. Outside the well the Schrödinger equation does not impose restrictions and the energy can have any value. But we know, from the study of the passage of a beam of particles through a potential step, that the discontinuity of the potential at the step provokes reflection even when the total energy of the particles is larger than the step, a situation where classically there would not be any difficulty for the passage of the particles. This reflection is partial and it becomes larger the closer the energy is closer to the height of the potential step. We can say that a particle with energy slightly positive is almost as confined as a particle inside the well. From

this fact results the existence of almost bound states of positive energy known as *quasi-stationary states* or *resonances*. These resonances appear as peaks in the excitation function, a peak at a given energy meaning that the energy coincides with a given resonance of the nucleus.

The existence of resonances can also be inferred from the properties of the wave function. We consider only elastic scattering, with the other channels closed. The external and internal wavefunctions are both sine functions, the first with wavenumber $k = \sqrt{2mE}/\hbar$ and the second with $K = \sqrt{2m(E - V_0)}/\hbar$. If E is small and V_0 is about -35 MeV, we have $K \gg k$. The internal and external parts should join at $r = R$ with continuous function and derivatives. As the internal frequency is much larger than the external one, the internal amplitude is quite reduced. Only at the proximity of the situation in which the derivative is zero there is a perfect matching between both and the internal amplitude is identical to the external one. The energy for which this happens is exactly the energy of resonance.

Resonances appear in the excitation function at relatively low energies, where the number of open channels is not very large and it is possible that to return to the entrance channel. To arrive at an expression of the cross section that describes a resonance, we rewrite 35 as,

$$u_l \sim \exp(-iKr) + b \exp(iKr), \quad (r < R), \quad (39)$$

this time containing a second part which takes into consideration the part of the wave that returns. This second part allows the existence of resonant scattering, where the incident particle is re-emitted with the same energy that it entered, after forming the compound nucleus. The complex amplitude b is always smaller than one, because there are no creation of particles in the region $< R$ in eq. 26.

The second parenthesis in the denominator of eq. 26 is never zero, since the numerator forces f_I to be always negative. If for a certain energy f_R vanishes, $\sigma_{r,0}$ passes by a maximum in that energy. We can tentatively identify these energies as being the energy of the resonances. Let us take the extreme case of a single resonance at the energy E_R , that is, $f_R = 0$ for $E = E_R$. We can expand f_R in a Taylor series in the neighborhood of a resonance, $f_R(E) = (E - E_R)(df_R/dE)_{E=E_R} + \dots$. Keeping just the first term of the expansion and using 24 and 26, we get

$$\sigma_{e,0} = \pi \bar{\lambda}^2 \left| \exp(2ikR) - 1 + \frac{i\Gamma_\alpha}{(E - E_R) + i\frac{\Gamma}{2}} \right|^2, \quad (40)$$

$$\sigma_{r,0} = \pi \bar{\lambda}^2 \frac{\Gamma_\alpha(\Gamma - \Gamma_\alpha)}{(E - E_R)^2 + \left(\frac{\Gamma}{2}\right)^2}, \quad (41)$$

where we define:

$$\Gamma_\alpha = -\frac{2kR}{(df_R/dE)_{E=E_R}} \quad \text{and} \quad \Gamma = \frac{2kR - 2f_I}{(df_R/dE)_{E=E_R}}. \quad (42)$$

The energy Γ that appears in 40, is the total width of the resonance, $\Gamma = \Gamma_\alpha + \Gamma_\beta + \dots$, i.e., the sum of the widths for all the possible processes of decay of the nucleus, starting from the resonant state. Γ_α is the entrance channel width, and $\Gamma - \Gamma_\alpha$ is the sum of the widths of all the exit channels except α . If we restrict the exit channels to a single channel β , or we denote β as the group of exit channels except α , eq. 41 is rewritten as

$$\sigma_{\alpha,\beta} = \pi \bar{\lambda}^2 \frac{\Gamma_\alpha \Gamma_\beta}{(E - E_R)^2 + \left(\frac{\Gamma}{2}\right)^2}, \quad (43)$$

which is the usual way of presenting the *Breit-Wigner formula*, which describes the form of the cross section close to a resonance. Let us recall that eq. 43 refers to an incident particle of $l = 0$, without charge and without spin. If the spins of the incident and target particles are s_a and s_A , respectively, and the incident beam is described by a single partial wave $l \neq 0$, one can show that the cross section of eq. 43 should be multiplied by the statistical factor $g = (2I+1)/(2s_a+1)(2s_A+1)$ where I is the quantum number of the total angular momentum $\mathbf{I} = \mathbf{s}_a + \mathbf{s}_A + \mathbf{l}$ of the compound nucleus. g reduces, naturally, to the unit in the case of zero intrinsic and orbital angular momenta.

If the exit channel is the same as the entrance channel α , the cross section should be obtained from 40 and its dependence in energy is more complicated because in addition to the resonant scattering there is the potential scattering, and the cross section 40 will contain an interference term between both. The presence of interference results in a peculiar aspect of the scattering cross section, which differs from the simple form 43 for the reaction cross section. This is seen in figure 8 that shows the forms that a resonance can take in the scattering cross section.

The region of energy where resonances show up can extend to 10 MeV in light nuclei but it ends well before this in heavy nuclei. Starting from this limit the increase in level density with energy implies that the average distance between levels is smaller than the width of the levels and individual resonances cannot be resolved experimentally. They form a continuum and this region is known as *continuum region*. The cross-section in this region fluctuates.

D. Statistical theory of nuclear reactions

The fluctuating behavior of low-energy nuclear reactions is due to the interference of the reaction amplitudes corresponding to the excitation of each of the overlapping states which vanish in the energy average of the cross-section since these amplitudes are complex functions with random modulus and phase. Calling $\sigma_N(c)$ the cross section for the formation of a compound nucleus in the entrance channel c , and using the *reciprocity theorem* which relates the cross-section $\sigma_{cc'}$ to the cross-

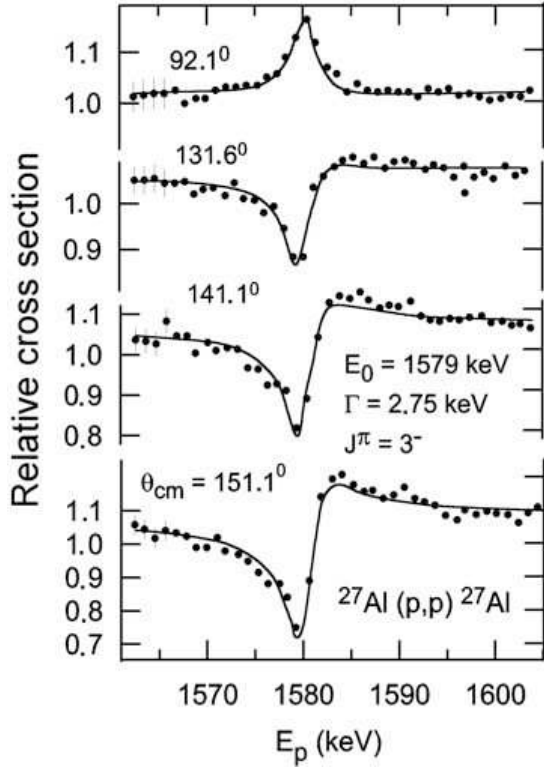


FIG. 8: Differential cross section at four angles for the elastic scattering of protons off ^{27}Al , in units of the Rutherford cross section, in the neighborhood of the 1579 keV resonance. For larger angles we have typical interference between the resonant scattering and the potential scattering [6].

section for the time-reversed process $c' \rightarrow c$, one gets

$$\sigma_{cc'}(E_{c'}) dE_{c'} = \sigma_{CN}(c) \times \frac{(2I_{c'} + 1) \mu_{c'} E_{c'} \sigma_{CN}(c') \omega(U_{c'}) dU_{c'}}{\sum_c \int_0^{E_c^{\max}} (2I_c + 1) \mu_c E_c \sigma_{CN}(c) \omega(U_c) dU_c} \quad (44)$$

where I_c is the angular momentum and μ_c is the reduced mass in channel c . Ejectiles with energy in the range $E_{c'}$ to $E_{c'} + dE_{c'}$ leave the residual nucleus with energy in the range $U_{c'}$ to $U_{c'} + dU_{c'}$ where $U_{c'} = E_{CN} - B_{c'} - E_{c'}$ and E_{CN} and $B_{c'}$ are respectively the compound nucleus energy and the binding energy of the ejectile in the compound nucleus. Eq. 44 is the *Weisskopf-Ewing formula* for the angle-integrated cross-sections [11]. To a good approximation, the level density $\omega(U) \propto \exp(U/T)$, so the ejectile spectrum given by the Weisskopf-Ewing theory is Maxwellian. It rises rapidly above the threshold energy, attains a maximum and then falls exponentially.

The Weisskopf-Ewing theory simple to use, but it has the disadvantage that it does not explicitly consider the conservation of angular momentum and does not give the angular distribution of the emitted particles. This is provided by the *Hauser-Feshbach theory* [12]. This theory takes into account the formation of the compound nucleus in states of different J and parity π . Let us consider

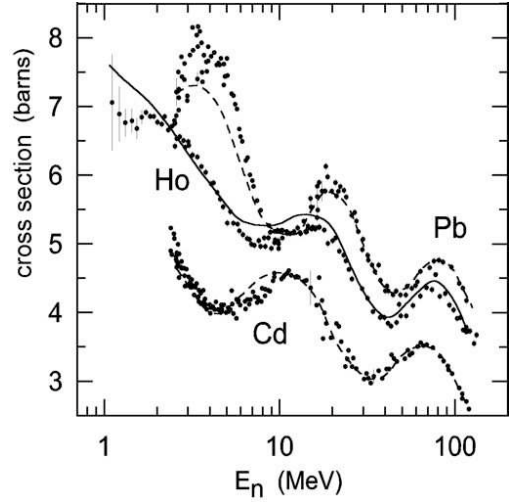


FIG. 9: Total cross section for neutrons incident on cadmium, holmium and lead, showing an oscillatory behavior. The curves for cadmium and lead are results of calculations with the optical model [7].

the case of a reaction leading from the initial channel c to a final channel c' . If there is no *pre-equilibrium emission*, one may identify the compound nucleus formation cross-section $\sigma_{CN} = \sum_{J,\pi} \sigma_{CN}^{J,\pi}$ with the optical model reaction cross-section $\sigma_R = \frac{\pi}{k^2} \sum_l (2l+1) T_l$, which, if the transmission coefficients $T_l = 1 - |\langle S_l \rangle|^2$ do not depend on J . $\langle S_l \rangle$ is the average value of the scattering amplitude over several overlapping resonances.

Using the above assumptions, the reciprocity theorem, and following a similar derivation as with the Ewing-Weisskopf theory, the cross-section for transition $c \rightarrow c'$ is given by the *Hauser-Feshbach* expression

$$\sigma_{cc'} = \frac{\pi}{k^2} \sum_J \frac{(2J+1)}{(2i_c+1)(2I_c+1)} \frac{\sum_{s,l} T_l(c) \sum_{s',l'} T_{l'}(c')}{\sum_c \sum_{s,l} T_l(c)} \quad (45)$$

The compound nucleus states may be both of positive and negative parity. Since parity is conserved, in evaluating (45), one must take into account that the parity of compound nucleus states and the parity of the residual nucleus states may impose restrictions to the values of the emitted particle angular momentum. Thus, positive parity compound nucleus states decay to positive parity states of the residual only by even angular momenta and to negative parity residual nucleus states by odd angular momenta.

E. The optical model

Expression 18 shows that if a particle is always absorbed when it reaches the nucleus, the total cross section falls monotonically with the energy and grows linearly with $A^{\frac{1}{2}}$. In figure 9 we see curves of total cross section

of neutron scattering showing an oscillatory behavior for its energy dependence as well as for the mass dependence of the target. Their presence is mainly due to interference phenomena between the part of the incident beam that passes through the nucleus and the part that passes around it [8].

The basis of the *optical model* was established by Herman Feshbach and collaborators in 1953 [9]. In this model the interaction between the nuclei in a reaction is described by a potential $U(r)$, with r being the distance between the center of mass of the two nuclei. One replaces the complicated interaction that a nucleon has with the rest of the nucleus with a potential that acts on the nucleon. The potential $U(r)$ includes a complex part that takes into account the absorption effects, i.e., the inelastic scattering. The nuclear scattering is treated in similar form as the scattering of light by a glass sphere and the name of the model derives of this analogy.

In its most commonly used form, the optical potential is written as the sum:

$$U(r) = U_R(r) + U_I(r) + U_D(r) + U_S(r) + U_C(r), \quad (46)$$

which contains parameters that can vary with energy and masses of the nuclei and that should be chosen by an adjustment to the experimental data. Obviously, the optical potential $U(r)$ will only make sense if these variations are small for neighboring masses or energies.

The first part of 46, $U_R(r) = -Vf(r, R, a)$, is real and represents a nuclear well with depth $-V$, being multiplied by a Woods-Saxon form factor $f(r, R, a) = [1 + \exp\{(r - R)/a\}]^{-1}$, where R is the radius of the nucleus and a measures the diffuseness of the potential, i.e., the width of the region where the function f is sensibly different from 0 or 1. V , R and a are treated as adjustable parameters.

The absorption effect or, in another way, the disappearance of particles from the elastic channel, is taken into account including the two following imaginary parts $U_I(r) = -iWf(r, R_I, a_I)$ and $U_D(r) = 4ia_IW_Ddf(r, R_I, a_I)/dr$. An imaginary part produces absorption. It is easy to see this for the scattering problem of the square well: if an imaginary part is added to the well, $U(r) = -V_0 - iW_0$ ($r < r_0$) and $U(r) = 0$ ($r > r_0$), it appears in the value of $K = [2m(E + V_0 + iW_0)]^{1/2}/\hbar$. This will produce an exponentially decreasing internal wavefunction. Thus, it corresponds to an absorption of particles from the incident beam.

U_I is responsible for the absorption in the whole volume of the nucleus, but U_D , built from the derivative of the function f , acts specifically in the region close to the nuclear surface. These two parts have complementary goals: at low energies there are no available unoccupied states for nucleons inside the nucleus and the interactions are essentially at the surface. In this situation $U_D(r)$ is important and $U_I(r)$ can be ignored. On the other hand, at high energies the incident particle has larger penetration and in this case the function $U_I(r)$ is important.

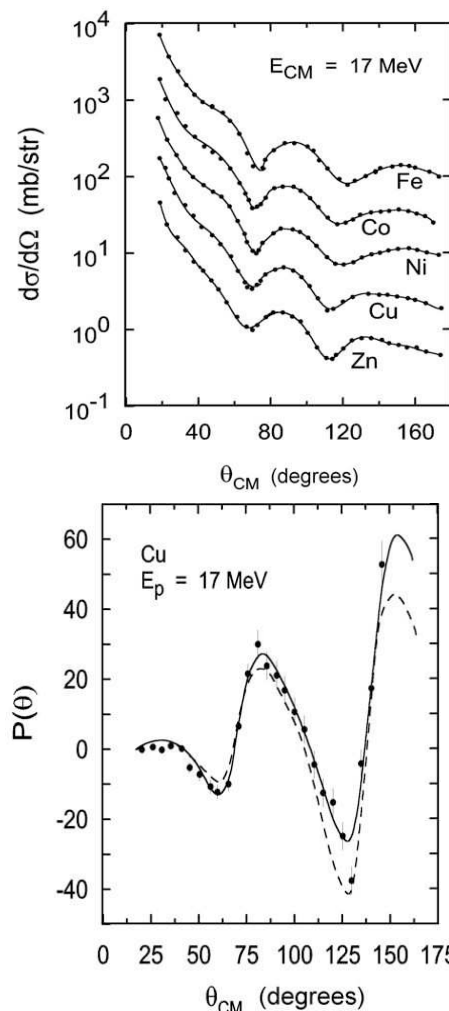


FIG. 10: (Top) Angular distribution of the elastic scattering of 17 MeV protons on nuclei in the region $Z = 26 - 30$. (Bottom) The polarization value 48 in the scattering of 9.4 MeV protons on copper. The curves are, in both cases, obtained with fits from the optical model [14].

As with the shell model potential, used in nuclear structure, a spin-orbit interaction term is added to the optical potential. This term, which is the fourth part of 46, is usually written in the form

$$U_S(r) = \mathbf{s} \cdot \mathbf{l} V_s \frac{1}{r} \frac{d}{dr} f(r, R_S, a_S). \quad (47)$$

\mathbf{s} is the spin operator and \mathbf{l} the angular orbital momentum operator. As with $U_D(r)$, the part $U_S(r)$ is only important at the surface of the nucleus since it contains the derivative of the form factor f . The values of V_S , R_S and a_S must be adjusted by experiment.

The presence of the term U_S is necessary to describe the effect of *polarization*. Through experiences of double scattering it can be verified that proton or neutron beams suffer strong polarization at certain angles. This means

that the quantity

$$P = \frac{N_c - N_b}{N_c + N_b}, \quad (48)$$

where N_c is the number of nucleons in the beam with spin up and N_b with spin down, has a value significantly different from zero at these angles. With the inclusion of U_S , the optical model is able to reproduce in many cases the experimental values for the polarization 48.

Finally, a term corresponding to the Coulomb potential is added to 46 whenever the scattering involves charged particles. It has the form

$$U_C(r) = \frac{Z_1 Z_2 e^2}{2R_c} \left(3 - \frac{r^2}{R_c^2} \right) \quad (r \leq R_c) \quad (49)$$

$$= \frac{Z_1 Z_2 e^2}{r} \quad (r > R_c), \quad (50)$$

where is assumed that the nucleus is a homogeneously charged sphere of radius equal to the *Coulomb barrier radius* R_c , which separates the regions of nuclear and Coulomb forces.

Figure 10 exhibits the result of the application of eq. 46 to the elastic scattering of 17 MeV protons on several light nuclei. The angular distribution is very well reproduced by the model, which also reproduces correctly the polarization 46 for copper as a function of the scattering angle.

The optical model has a limited set of adjustable parameters and is not capable to describe abrupt variations in the cross sections, as it happens for isolated resonances. However, it can do a good description of the cross sections in the presence of the oscillations of large width in the continuous region, as it treats these as wave phenomena.

IV. DIRECT REACTIONS

Direct reactions becomes more probable as one increases the energy of the incident particle: the wavelength associated to the particle decreases and localized areas of the nucleus can be “probed” by the projectile. In this context, peripheral reactions, where only a few nucleons of the surface participate become important. Direct reactions happen during a time of the order of 10^{-22} s. Reactions with formation of compound nuclei can be up to six orders of magnitude slower. A reaction type at a given energy is not necessarily exclusive; the same final products can be obtained, part of the events in a direct way, other parts through the formation and decay of a compound nucleus.

There are two characteristic types of direct reactions. In the first the incident particle scatters inelastically and the transferred energy is used to excite a collective mode of the nucleus. Rotational and vibrational bands can be studied in this way. The second type involves a modification in the nuclear composition. Examples are transfer of nucleons, as *pick-up* and *stripping* reactions. An important reaction of the latter kind is a *knock-out* reaction

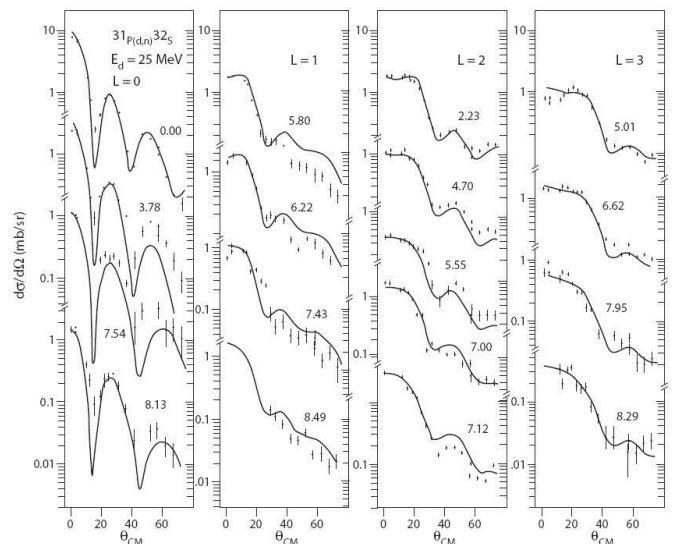


FIG. 11: Angular distribution of the reaction $^{31}\text{P}(d,n)^{32}\text{S}$, with the transfer of a proton to several states of ^{32}S . The curves are results of DWBA calculations for the indicated l values [15].

where the incident particle knocks out a particle of the target nucleus and continues in its path, resulting in three reaction products. Reactions with nucleon exchange can also be used to excite collective states. An example is a pick-up reaction where a projectile captures a neutron from a deformed target and the product nucleus is in an excited state belonging to a rotational band.

Direct reactions exhibit a peculiar form of angular distribution, which allows us to extract information on the reaction mechanism with the employment of simple models. Typical examples are the stripping reactions (d,n) and (d,p), where the angular distribution of the remaining nucleon presents a forward prominent peak and smaller peaks at larger angles, with the characteristic aspect of a diffraction figure.

Figure 11 shows experimental results for the reaction $^{31}\text{P}(d,n)^{32}\text{S}$ [15]: angular distributions of the detected neutrons corresponding to each energy level of ^{32}S are exhibited for several angular momentum. We see that the behavior of the cross sections is in agreement with qualitative predictions: the curves exhibit a first peak at a value of θ that grows with l . Other smaller peaks occur as θ increases. The increase of θ_l with l is an important characteristic that can be used to identify the value of the transferred momentum in a given angular distribution.

We consider an initial quantum state with particles of mass m_a hitting a target A of mass m_A . The final quantum state are particles of mass m_b moving away from nucleus B of mass m_B . The differential cross section for the process is given by

$$\frac{d\sigma}{d\Omega} = \frac{m_a m_b k_b}{(2\pi\hbar^2)^2 k_a} |V_{fi}|^2, \quad (51)$$

involving the matrix element

$$V_{fi} = \int \Psi_b^* \Psi_B^* \Psi_\beta(\mathbf{r}_\beta) V \Psi_a \Psi_A \Psi_\alpha(\mathbf{r}_\alpha) d\tau. \quad (52)$$

$\Psi_a, \Psi_b, \Psi_A, \Psi_B$ are the internal wavefunctions of the nuclei a, b, A and B. Ψ_α, Ψ_β are the wavefunctions of the relative motion in the entrance channel α and in the exit channel β . The integration volume $d\tau$ spans the coordinates of all particles. V is the perturbation potential that causes the “transition” from the entrance to the exit channel.

The use of plane waves for Ψ_α and Ψ_β in eq. 52 is known as *first Born approximation*. With it we can arrive to an approximate expression for the behavior of the differential cross section. As the nuclear forces are of short range, one can restrict the integral 52 to regions where $\mathbf{r}_\alpha \cong \mathbf{r}_\beta = \mathbf{r}$. This leads to

$$V_{fi} \cong \int d\mathbf{r} \exp(i\mathbf{k} \cdot \mathbf{r}) \left\{ \int \Psi_b^* \Psi_B^* V \Psi_a \Psi_A d\tau' \right\}, \quad (53)$$

where $\mathbf{k} = \mathbf{k}_\alpha - \mathbf{k}_\beta$. The global variables in $d\tau$ were separated into variables $d\mathbf{r}$ and $d\tau'$.

Expanding the plane wave in a Legendre polynomial series, we obtain

$$V_{fi} \cong \sum_{l=0}^{\infty} i^l (2l+1) \int j_l(kr) P_l(\cos\theta) F(\mathbf{r}) d\mathbf{r}, \quad (54)$$

where $F(\mathbf{r}) = \int \Psi_b^* \Psi_B^* V \Psi_a \Psi_A d\tau'$ contains all the internal properties and is known as the *form factor* of the reaction. The action of V is restricted to the surface of the nucleus: outside the nucleus the action of V is limited by the short range of the nuclear forces and inside the nucleus there is a strong deviation to the absorption channel. Expression 54 becomes $V_{fi} \cong \sum_{l=0}^{\infty} c_l j_l(kR)$, where the coefficients c_l contain information on the form factor $F(\mathbf{r})$. The index l can be identified as the angular momentum transferred and, for a reaction that involves a single value of l , we can write for the differential cross section:

$$\frac{d\sigma}{d\Omega} \propto |j_l(kR)|^2, \quad (55)$$

where the dependence in θ is contained in

$$k^2 = k_\alpha^2 + k_\beta^2 - 2k_\alpha k_\beta \cos\theta. \quad (10.82)$$

We have an oscillatory behavior for the angular distribution, the maxima separated by π from each other in the axis kR .

The Born approximation with plane waves predicts for certain cases the correct place of the first peaks in the angular distribution but without reproducing correctly the intensities. A considerable progress can be done in the perturbative calculations if, instead of plane waves in 52, we use *distorted waves* that contain, besides the plane wave, the part dispersed elastically by the optical

potential of the target. The Born approximation with distorted waves, or DWBA (*distorted wave Born approximation*), became a largely employed tool in the analysis of experimental results of direct reactions. With it one can try to extract with a certain reliability the value of the angular momentum l transferred to the nucleus in a stripping or pick-up reaction. An example of this is the already mentioned stripping reaction, $^{31}\text{P}(\text{d,n})^{32}\text{S}$, for deuterons of 25 MeV. For the energy levels shown in figure 11 the assignments of the value of l for the level is, in most cases, univocal.

The angular momentum l transferred in a direct reaction generally modifies the value of the total angular momentum of the nucleus. If J_i is the spin of the target nucleus, the spin J_f of the product nucleus is limited to the values

$$\left| |J_i - l| - \frac{1}{2} \right| \leq J_f \leq J_i + l + \frac{1}{2}, \quad (56)$$

and the initial and final parities obey the relationship $\pi_i \pi_f = (-1)^l$. Eq. 56 allows, with the knowledge of the target nucleus and of the transferred angular momentum, the determination of the parity of the product state formed and is a tool for the determination of its spin.

The knowledge of the transferred angular momentum value in a direct reaction opens the possibility to test the predictions of the shell model for the structure of nuclei. In a direct reaction one assumes that the nucleon is located in an orbit of the nucleus with the same angular momentum as the transferred momentum in the reaction. In almost all cases studied with direct reactions the value of the assigned l corresponds exactly to the predicted by the shell model. We know, however, that the real situation is more complicated, due to the presence of the residual interactions that give place to configuration mixing. As result, the cross section for the formation of a state i of the product nucleus is related to that calculated with DWBA for the formation from a single-particle state by

$$\left(\frac{d\sigma}{d\Omega} \right)_{\text{exp}} = \frac{2J_B + 1}{2J_A + 1} \mathcal{S}_{ij} \left(\frac{d\sigma}{d\Omega} \right)_{\text{DWBA}}, \quad (57)$$

where the *spectroscopic factor* \mathcal{S}_{ij} measures the weight of the configuration j used in the DWBA calculation, in the final state i , with the sum-rule

$$\sum_j \mathcal{S}_{ij} = n_i. \quad (58)$$

The sum 58 embraces all the nucleons in the configurations j of the product nucleus. The statistical weight $(2J_B + 1)/(2J_A + 1)$ that appears in the DWBA calculation involving the angular momentum of the target nucleus J_A and final nucleus J_B , is explicitly given in 58.

V. HEAVY ION REACTIONS

A. Types and properties

Heavy ion reactions (with $A > 4$) can be separated into 3 major categories.

1) Due to their large charge, two heavy nuclei feel a strong mutual Coulomb repulsion. To produce a nuclear reaction the projectile needs enough energy to overcome the Coulomb barrier. For a very heavy target, as ^{238}U , it is necessary about 5 MeV per nucleon. Then the wavelength of the projectile is small compared with the dimensions of the nuclei and classical and semi-classical methods become useful in the description of the reaction.

2) The projectile carries a large amount of angular momentum and a good part of it can be transferred to the target in the reaction. Rotational bands with several dozens of units of angular momentum can be created. In fact, heavy ion reactions are the best suited to feed high spin levels.

3) Direct reactions and formation of compound nucleus are also common processes in reactions with heavy ions. But some peculiarities of these are not found in reactions with projectile nucleons. One of these processes can be understood as intermediate between a direct reaction and the formation of a compound nucleus. Fusion does not occur but projectile and target pass a relatively long time under the mutual action of the nuclear forces. Nuclear matter is exchanged between both and there is a strong heating of the two nuclei, with a large transfer of kinetic energy to the internal degrees of freedom. These are the *deep inelastic collisions*.

The kind of process that prevails depends upon the distance of closest approach d between the projectile and target. If this distance is sufficiently large only the long range Coulomb interaction acts and, for a classical hyperbolic trajectory, d is related to the impact parameter b and to the energy E of the projectile by $d = a/2 + [(a/2)^2 + b^2]^{1/2}$ where a is the distance of closest approach in a head-on collision. It is this is related to E by $a = Z_1 Z_2 e^2 / 4\pi\epsilon_0 E$.

Experimentally, the variable under control is the energy E of the projectile and, for E sufficiently large, d can be small enough to enter the range of nuclear forces. Collisions near this limit are called *grazing collisions* and are characterized by values of b_{graz} and d_{graz} . Assuming that there is always reaction when $b < b_{graz}$, the reaction cross section σ_r can be determined geometrically by $\sigma_r = \pi b_{graz}^2$. The experimental determination of σ_r allows to establish the value $d_{graz} = 0.5 + 1.36(A_1^{1/3} + A_2^{1/3})$ showing that the distance of grazing collision is somewhat larger than that deduced from two touching spheres (1.36 fm $>$ $r_0 = 1.2$ fm).

When the impact parameter is close to b_{graz} one expects nuclear reactions of short duration, without the contribution of the compound nucleus formation. Such reactions are elastic and inelastic scattering and transfer

of few nucleons. When the incident energy is sufficiently high, small values of b can lead to the projectile penetrating the target. Depending on the energy and on the involved masses, the reaction can end in one of the processes below:

a) *Fusion* - is the preferred process when one has light nuclei and low energy. There is the formation of a highly excited compound nucleus that decays by evaporation of particles and γ -radiation emission, leading to a cold residual nucleus. If the energy in the CM is close to the Coulomb barrier energy the cross section of compound nucleus formation starting from two nuclei is practically equal to the reaction cross section.

b) *Fission* - When the compound nucleus is heavy the fission process competes strongly with the evaporation of particles in each stage of the evaporation process. A very heavy compound nucleus with a large excitation energy has a very small probability of arriving to a cold residual nucleus without fission at some stage of the de-excitation. The role of the angular momentum l transmitted to the target nucleus is also essential. The fission barrier decreases with the increase of l and for a critical value l_{crit} the barrier ceases to exist. A nucleus with angular momentum greater than l_{crit} suffers immediate fission and this is also a limiting factor in the production of super-heavy elements.

c) *Deep inelastic collision (DIC)* - is a phenomenon characteristic of reactions involving very heavy nuclei ($A > 40$) and with an incident energy of 1 MeV to 3 MeV above the Coulomb barrier. In DIC the projectile and the target spend some time under mutual action, exchanging masses and energy but without arriving to the formation of a compound nucleus. The projectile escapes after transferring part of its energy and angular momentum to its internal degrees of freedom and to the target, with values reaching 100 MeV and $50\hbar$.

One of the most interesting aspects of DIC is the correlation between the energy dissipated in the collision and the scattering angle in the center of mass. Let us look at figure 12(top). The trajectory 1 shows the projectile with an impact parameter that leads it out of the range of nuclear forces. The Coulomb scattering angle will become larger as the impact parameter decreases. In a graph as in figure 12(bottom), where one plots the final energy against the scattering angle, trajectories of type 1 are located in the upper branch, where there is no dissipation and the initial kinetic energy stays unaffected. This upper branch has a maximum value for the scattering angle. At a smaller impact parameter the nuclear attractive force begins to act and, with that the effects of dissipation of DIC. A given Coulomb scattering angle θ can also be reached by the combination of the nuclear and Coulomb forces. Only that now there is loss of energy and the events are located in the branch 2 of figure 12(b). There still is no one-to-one correspondence between angle and energy because an infinite number of trajectories can lead to the same angle θ . The branch 2 should be understood as a line of maxima in a three-

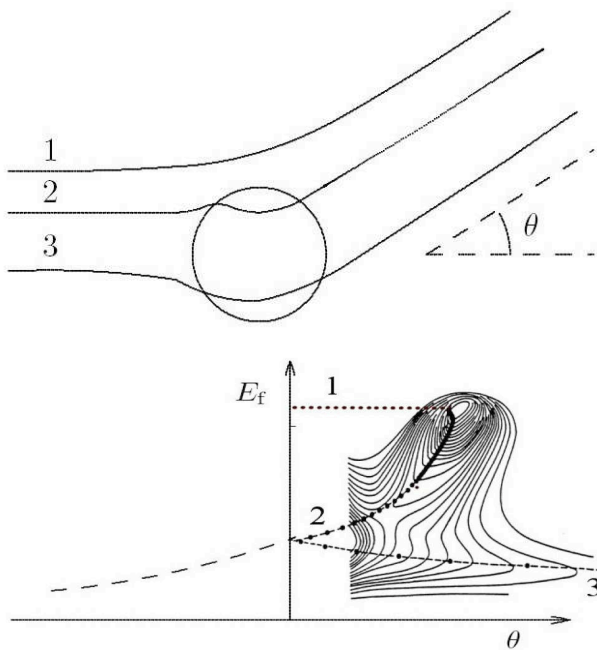


FIG. 12: (Top) Reactions with different impact parameters leading to the same scattering angle θ . (Bottom) Lines of maxima in topographical diagrams of the final energy against the scattering angle.

dimensional representation (called *Wilczynski diagram*) where the axis perpendicular to the paper is proportional to the cross section $d^2\sigma/dEd\theta$. The same angle θ can also be obtained by the trajectory 3, with a longer interaction time between the nuclei and a larger dissipation. As now the projectile is deflected towards the nucleus, the scattering angle would be formally $-\theta$ but, as there is no experimental distinction between θ and $-\theta$, these events appear as an independent ramification in the lower part of the diagram.

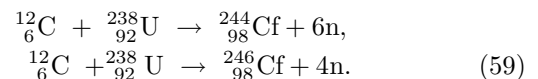
B. Superheavy elements

The heaviest element found in the nature is ${}_{92}^{238}\text{U}$. It is radioactive, but it survived since its formation in supernovae explosions because it has a decay half-life of the order of the age of the Earth. Elements with larger atomic number (transuranic) have shorter half-lives and have disappeared. They are created artificially through nuclear reactions using heavy elements as target. Initially, the projectiles used were light particles: protons, deuterons, α -particles and neutrons. The use of neutron is justified because the β^- -emission of the compound nucleus increases the value of Z and it was in this way [19] that the first transuranic element, the neptunium, was obtained: $n + {}_{92}^{238}\text{U} \rightarrow {}_{93}^{239}\text{U} \rightarrow {}_{93}^{239}\text{Np} + \beta^-$.

Reactions with light particles can produce isotopes up to mendelevium ($Z = 101$), but it is not possible to go

beyond that; the half-lives for α -emission or spontaneous fission become extremely short, turning impracticable the preparation of a target. The alternative is to place a heavy element under the flux of very intense neutrons. This can be done using special reactors or using the rest material of nuclear explosions. The elements einsteinium ($Z = 99$) and fermium ($Z = 100$) were discovered in this way in 1955 but the increasing competition that the beta decay has with alpha decay and with spontaneous fission prevents this method to be used for larger Z .

Starting in 1955 heavy ion accelerators began to deliver beams with high enough intensity and energy to compete in the production of transuranic isotopes. The first positive result was the production of two californium isotopes ($Z = 98$) in the fusion of carbon and uranium nuclei:



This opened the possibility of reaching directly the nucleus one wants to create from the fusion of two smaller nuclei. The difficulty of such task is that the cross sections for the production of heavy isotopes are extremely low. As example, the reaction ${}_{22}^{50}\text{Ti} + {}_{82}^{208}\text{Pb} \rightarrow {}_{104}^{257}\text{Rf} + n$, which produces the element rutherfordium, has a cross section of only 5 nb. A small increase in the charges reduces drastically this value: the cross section for the fusion reaction ${}_{26}^{58}\text{Fe} + {}_{82}^{208}\text{Pb} \rightarrow {}_{108}^{265}\text{Hs} + n$ is 4 pb. As comparison, the typical cross sections of DIC for heavy nuclei are in the range 1-2 b.

In spite of the experimental refinement that these low cross sections demand, one is able to produce isotopes with charge as heavy as $Z = 118$. The understanding of the mechanisms that lead to fusion is, however, not fully understood. According to the traditionally accepted model, the fusion of two nuclei proceeds in two stages: the formation of a compound nucleus and the de-excitation of the compound nucleus by evaporation of particles, preferentially neutrons. The difficulties for the materialization of the process in very heavy nuclei reside in both stages [20].

VI. ELECTROMAGNETIC PROBES

A. Coulomb Excitation

Coulomb excitation is a inelastic scattering process in which a nucleus excites another nucleus with its electromagnetic field V . This field can be decomposed in terms of a series of multipoles, e.g. $E1, E2, M1, \dots$, which carry well defined angular momenta and parities. At low bombarding energies $E2$ (quadrupole) excitations are more common, while at higher energies $E1$ excitations dominate. As an example of a low energy reaction, let us consider the excitation of a quadrupole state in a head-on collision below the Coulomb barrier, i.e. for a situation in which the projectile decelerates as it approaches the target and stops before reaching the range

of the nuclear interaction, reaccelerating backwards after that. The differential cross section is given by the product of the Rutherford differential cross section at 180° and the probability of transition of the target from state i to state f , along the trajectory, measured by the square of

$$\frac{d\sigma}{d\Omega}\Big|_{\theta=180^\circ} = \frac{d\sigma_R}{d\Omega}\Big|_{\theta=180^\circ} \times |a_{if}|^2. \quad (60)$$

The square of a_{if} measures the transition probability from i to f and this probability should be integrated along the trajectory. A simple calculation for a_{if} can be done in the case of the excitation from the ground state $J = 0$ of a deformed nucleus to an excited state with $J = 2$. The perturbation V comes, in this case, from the interaction of the projectile charge $Z_P e$ with the quadrupole moment of the target nucleus. This quadrupole moment works as an operator that acts between the initial and final states, i.e.

$$V = \frac{1}{2} \frac{Z_P e^2 Q_{if}}{r^3}, \quad (61)$$

where r is the projectile-target separation distance and

$$Q_{if} = \sum_i \int \Psi_f^* (3z_i^2 - r_i^2) \Psi_i d\tau, \quad (62)$$

where the sum extends to all protons at the positions $r_i = (x_i, y_i, z_i)$ in the target. The amplitude is then given by

$$a_{if} = \frac{4Q_{if}E^2}{3Z_P e^2 \hbar v_0 Z_T^2}. \quad (63)$$

Using eq. 60 for the Rutherford differential cross section at $\theta = 180^\circ$, we obtain

$$\frac{d\sigma}{d\Omega}\Big|_{\theta=180^\circ} = \frac{mE|Q_{if}|^2}{18\hbar^2 Z_T^2}, \quad (64)$$

which is an expression that is independent of the charge of the projectile. It is, on the other hand, proportional to the mass of the projectile, indicating that heavy ions are more effective for Coulomb excitation.

The quadrupole moment operator Q_{if} uses the wavefunctions Ψ_i and Ψ_f of the initial and final states. If those two wavefunctions are similar, as is the case of an excitation to the first level of a rotational band, the operator Q_{if} can be replaced by the intrinsic quadrupole moment Q . The expression translates, in this way, the possibility to evaluate the quadrupole moment from a measurement of the cross section. This has been indeed a major spectroscopic tool for determining quadrupole momenta (and transitions) along the nuclear chart.

B. Photonuclear reactions and giant resonances

A photonuclear reaction is a reaction resulting from the interaction of the electromagnetic radiation with a

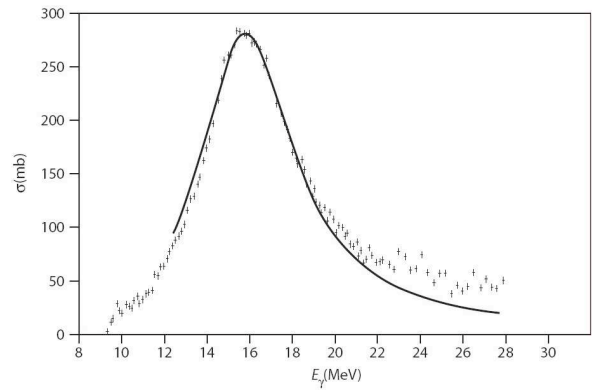


FIG. 13: Giant resonance in the absorption of photons by ^{120}Sn [21].

nucleus. Therefore, one can access information which are complementary to Coulomb excitation (and vice-versa).

When the energy of the photon is located above the separation energy of a nucleon, the cross section of photoabsorption reveals the presence of characteristic sharp resonances. But when the incident energy reaches the range of 15-25 MeV, a new behavior appears in the cross section, with the presence of a wide and large peak, called *giant electric dipole resonance* ($E1$ excitation). Figure 13 exhibits the excitation function of photoabsorption of ^{120}Sn at photon energies around the electric dipole giant resonance at 15 MeV.

The giant resonance occurs in nuclei along the whole periodic table, with the resonance energy decreasing was $E_{GDR} \simeq 80/A^{1/3}$ for $A > 20$. Their widths are almost all in the range between 3.5 MeV and 5 MeV. In few cases they can reach 7 MeV. They are a collective excitation, i.e., an excitation involving many nucleons at once. The time-varying electric field of the photon is very effective in inducing collective oscillations of protons against neutrons.

The giant electric dipole (GDR) resonance arises from an excitation that transfers by one unit of angular momentum to the nucleus ($\Delta l = 1$). If the nucleus is even-even it is taken to a 1^- state. The transition also changes the isospin of 1 unit ($\Delta T = 1$) and, due to that, it is also called *isovector resonance*. The photon can excite less effectively, but still with appreciable cross sections, giant isoscalar resonances, with $\Delta T = 0$. But electric quadrupole ($\Delta l = 2$) and electric monopole ($\Delta l = 0$) are observed mostly in reactions with charged particles. In a giant electric quadrupole resonance the nucleus oscillates between an spherical (assuming that this is the form of the ground state) to an ellipsoidal form. If protons and neutrons vibrate in phase, we have an isoscalar resonance ($\Delta T = 0$) and if they are oscillate in opposite phase we have an isovector resonance ($\Delta T = 1$). The giant monopole resonance is a very special case of nuclear excitation where the nucleus contracts and expands radially, maintaining its original form but changing its

volume. It is also called *breathing mode*. It can also happen in isoscalar and isovector forms. It is an important way to study the *compressibility of nuclear matter*.

Besides electric giant resonances, associated to a variation in the form of the nucleus, magnetic giant resonances exist, involving *spin vibrations*. In these, nucleons with spin up move out of phase with nucleons with spin down. The number of nucleons involved in the process cannot be very large because it is limited by the Pauli principle. The magnetic resonances can also separate into isoscalar resonances, where protons and neutrons of same spin vibrate against protons and neutrons of opposite spin, and isovector, where protons with spin up and neutrons with spin down vibrate against their corresponding partners with opposite spins. The last cases, are effectively probed in charge-exchange reactions, i.e. when the projectile charge changes to $Z-1$ or $Z+1$, as in (d,p) and (d,n). They are known as *giant Gamow-Teller resonances*.

Giant resonances can also be produced in an excited nucleus, a case known as the Brink-Axel hypothesis [22]. A special case is when two giant resonances are excited in the same nucleus. The double giant dipole resonance (or *multiphonon giant resonance* was observed for the first time in reactions with double charge exchange induced by pions in the ^{32}S [23]. But Coulomb excitation proved to be their best probe, as shown theoretically in refs. [24, 25].

C. Electron scattering

Electron scattering experiments have provided a rich database on most stable or long-lived nuclei. Electrons are structureless point-like objects that only interact electromagnetically. Therefore, electron scattering avoids the complexity of the strong interaction between the projectile and the target, and provides clean information about the charge distribution in the nucleus.

Considering relativity and the spin of the electrons, the differential cross section for elastic scattering by spinless point-like nuclei can be expressed by the *Mott scattering formula* (for simplicity, we use $\hbar = c = 1$ units):

$$\left(\frac{d\sigma}{d\Omega}\right)_{Mott} = \frac{Z_T^2 e^4 \cos^2(\theta/2)}{4p_0^2 \sin^4(\theta/2) [1 + (2p_0/M) \sin^2(\theta/2)]} \quad (65)$$

where $Z_T e$ and M are the charge and mass of the target nucleus respectively, and p_0 is the momentum of the incoming electron. Since the nucleus is not a point-like particle, the formula is modified by adding the nuclear electric and magnetic form factors, which contain information of the charge and magnetization distributions inside the nucleus.

The *Rosenbluth formula* accounts for the electron spin and explicitly expresses the cross section for arbitrary

nuclei as

$$\left(\frac{d\sigma}{d\Omega}\right)_{Mott} = \left(\frac{d\sigma}{d\Omega}\right)_{Mott} \left\{ A_0(q^2) + B_0(q^2) \left[\frac{1}{2} + \left(1 + \frac{q^2}{4M^2}\right) \tan^2(\theta/2) \right] \right\},$$

where $q^2 = (\mathbf{p}_f - \mathbf{p}_i)^2 - (E_f - E_i)^2$ is the 4-momentum transfer squared, where \mathbf{p}_i (\mathbf{p}_f) and E_i (E_f) are the electron incoming (outgoing) momentum and energy. $A_0(q^2)$ and $B_0(q^2)$, are functions of q^2 , are the form factors associated with the charge and magnetization distribution of the nucleus respectively. For a spin-0 nucleus:

$$A_0(q^2) = \frac{G_E^2(q^2)}{1 + q^2/4M^2} \quad \text{and} \quad B_0(q^2) = 0, \quad (66)$$

where $G_E(q^2)$ is the *Sachs charge form factor*, and the factor $1 + q^2/4M^2$ is the kinematical recoil correction. For $q \rightarrow 0$, $q^2 \approx \mathbf{q}^2$, where \mathbf{q} is the three-momentum transfer, and to leading order in powers of \mathbf{q} :

$$G_E(q^2) \simeq G_E(\mathbf{q}^2) = \int \rho_T(\mathbf{r}) e^{i\mathbf{q}\cdot\mathbf{r}} d^3r. \quad (67)$$

One thus sees that electron scattering is related to the Fourier transform of the nuclear charge density, $\rho_T(\mathbf{r})$. If the function $G_E(\mathbf{q}^2)$ is mapped for a sufficient number of momentum transfers \mathbf{q}^2 the Fourier transform can be inverted and $\rho_T(\mathbf{r})$ can be mapped with precision. For heavy elements ($A > 10$), this technique shows that the charge radius is closely proportional to $1.12 A^{1/3}$ fm, where A is the nuclear mass number. This indicates the density saturation for the nuclear matter.

When $\mathbf{q}^2 = 0$, inelastic electron scattering probes the same multipolarity transitions ($E1$, $E2$, \dots) as in Coulomb excitation or with real photons. However, in contrast to the later probes, electron scattering also provides information on nuclear excitations for cases in which $\mathbf{q}^2 \neq 0$. This is useful in many aspects. For example, at high momentum transfers, the momentum transfer \mathbf{q} can be absorbed by a nucleon in the nucleus which acquires an energy of the order of $\mathbf{q}^2/2m_N^*$, thus probing the effective mass m_N^* of a nucleon in the nucleus. This is of relevance to understand the effects of nucleon-nucleon interactions in the nuclear environment. The q -region where this occurs is termed by *quasi-free scattering*. As electrons can penetrate the nuclei, they can also more effectively probe monopole (or breathing mode) excitations of the nuclei, a case in which the nuclear mass distribution vibrates radially. This is of importance for determining the *compressibility modulus* of the nuclear matter. Finally, in high-energy electron scattering the electron can penetrate deeply inside the nucleons and probe the spin and charge distributions of quarks and gluons inside the nucleon [26].

VII. RELATIVISTIC NUCLEAR COLLISIONS

A. Transport theories and equation of state

As the bombarding energy in nucleus-nucleus collisions increases the structure aspects of the nuclei become less relevant. Except for the bulk properties of the nuclei (size and number of nucleons), the physics involved is primarily due to the individual, and sometimes collective, hadronic collisions. Several theoretical tools are used to describe these reactions, and in particular we quote (a) *time-dependent Hartree-Fock* (TDHF), (b) *antisymmetrized molecular dynamics* (AMD), (c) *Boltzmann-Uehling-Uhlenbeck* (BUU, etc.

At intermediate energies of $E_{lab} \sim 100 - 1000$ MeV/nucleon the nucleons and the products of their collisions can be described individually and their propagation can be described by semiclassical equations. One of such equations, and perhaps the most popular in such studies, is the so-called *Boltzmann-Uehling-Uhlenbeck* (BUU) equation:

$$\begin{aligned} \frac{\partial f}{\partial t} + \left(\frac{\mathbf{p}}{m} + \nabla_{\mathbf{p}} U \right) \cdot \nabla_{\mathbf{r}} f - \nabla_{\mathbf{r}} U \cdot \nabla_{\mathbf{r}} f = \\ \int d^3 p_2 \int d\Omega \sigma_{NN}(\Omega) |\mathbf{v}_1 - \mathbf{v}_2| \\ \times \{ f'_1 f'_2 [1 - f_1] [1 - f_2] - f_1 f_2 [1 - f'_1] [1 - f'_2] \}, \quad (68) \end{aligned}$$

If dN is the number of particles in the volume element d^3r and whose momenta fall in the momentum element d^3p at time t , then the distribution function $f(\mathbf{r}, \mathbf{p}, t)$ is given by $dN = f(\mathbf{r}, \mathbf{p}, t) d^3r d^3p$. Thus the BUU equation is an equation for the distribution function $f(\mathbf{r}, \mathbf{p}, t)$. To account for the effect of each particle interacting with all others, one introduces the concept of *mean-field*, $U(\mathbf{r}, \mathbf{p}, t)$. This mean-field exerts a force on each particle, given by $-\nabla_{\mathbf{r}} U(\mathbf{r}, \mathbf{p}, t)$. Also, the momentum dependence of the potential introduces a dependence through the derivative $-\nabla_{\mathbf{p}} U(\mathbf{r}, \mathbf{p}, t)$.

Due to the nucleon-nucleon collisions, the distribution function within $d^3r d^3p$ can also be modified by nucleons leaving (or entering) this volume. This is taken care by the *collision term*, i.e. the right-hand-side of the BUU equation. σ_{NN} is the nucleon-nucleon differential scattering cross section, \mathbf{v}_1 and \mathbf{v}_2 are the velocities of two colliding nucleons. The first factor inside braces are for collisions populating the volume element and the second term for those depleting it. The factors $(1 - f)$ account for Pauli blocking of final occupied states. The integrals average over scattering angle and over all collisions within $d^3r d^3p$. The BUU equation falls in the category of what one calls *quantum transport theories*. Hadronic transport theories have been quite successful in applications, describing a multitude of measured particle spectra.

Eq. (68) needs as basic ingredients the mean field U and the cross section σ_{NN} . Because these two quantities are related to each other, one should in principle derive them in a self-consistent microscopic approach, as in the

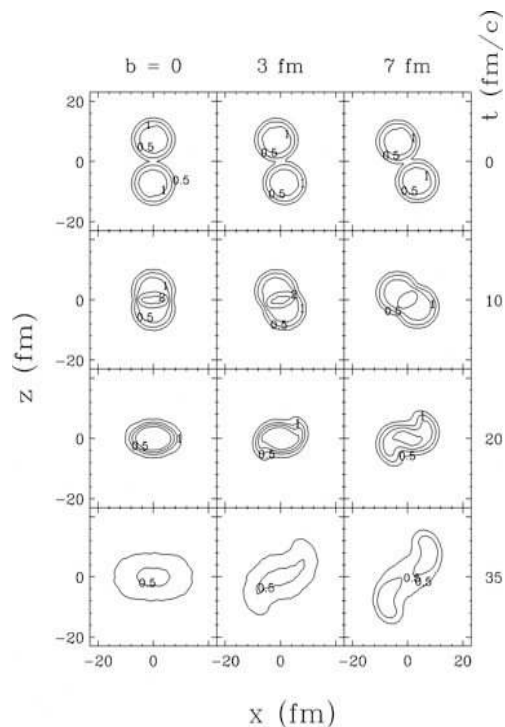


FIG. 14: - Contour plots of baryon density in the reaction plane in Au + Au collisions at 400 MeV/nucleon. The displayed contour lines are for the densities $\rho/\rho_0 = 0.1, 0.5, 1, 1.5,$ and 2 [27].

Brueckner theory. However, in practice the simulations are often done with a phenomenological mean field and free nuclear cross sections.

An important ingredient in the transport theory calculations is the compressibility K of nuclear matter, which refers to the second derivative of the compressional energy E with respect to the density:

$$K = 9\rho^2 \frac{\partial^2}{\partial \rho^2} \left(\frac{E}{A} \right). \quad (69)$$

This is an important quantity, e.g., for nuclear astrophysics. Supernova models might or not lead to explosions depending on the value of K . The central collisions of heavy nuclei are one of the few probes of this quantity in the laboratory. The dependence of the calculations on K follow from the dependence of the mean field potential U ($U \sim E/A +$ kinetic energy terms) on the particle density ρ . A typical parametrization for U is the Skyrme parametrization $U = a\rho/\rho_0 + b(\rho/\rho_0)^\sigma$.

The output of eq. (68) is the distribution function $f(\mathbf{r}, \mathbf{p}, t)$, which allows one to calculate many properties of heavy-ion collisions. Let us quote *collective flows*, proton and neutron production rates, (sub-threshold and above threshold) pion and kaon yields, etc. Combining

eq. (68) with a *phase-space coalescence model*, one can also calculate such quantities as exclusive flows and intermediate fragment formations.

The dynamics of the central high-energy reactions can be broken down into several stages. Baryon-density contour-plots are shown in fig. 14 for 400 MeV/nucleon Au+Au collisions at $b = 0$, which will serve to illustrate our points.

Following an initial interpenetration of projectile and target densities, the NN collisions begin to thermalize matter in the overlap region making the momentum distribution there centered at zero momentum in the CM. The density in the overlap region rises above normal and a disk of excited and compressed matter forms at the center of the system. More and more matter dives into the region with compressed matter that begins to expand in transverse directions. At late stages, when the whole matter is excited, transverse expansion predominates.

B. Kinematics

In relativistic nucleus-nucleus collisions other definitions are best suited for discussing relations between energies, momenta and angles. The *rapidity* is a variable frequently used to describe the behavior of particles in inclusively measured reactions. It is defined by

$$y = \frac{1}{2} \ln \left(\frac{E + p_{\parallel}}{E - p_{\parallel}} \right) \quad (70)$$

which corresponds to $\tanh y = \frac{p_{\parallel}}{E}$, where y is the rapidity, p_{\parallel} is the longitudinal momentum along the direction of the incident particle, E is the energy, both defined for a given particle. The accessible range of rapidities for a given reaction is determined by the available center-of-mass energy and all participating particles' rest masses. One usually gives the limit for the incident particle, elastically scattered at zero angle:

$$|y_{\max}| = \ln \left[\frac{E + p}{m} \right] = \ln(\gamma + \gamma\beta) \quad (71)$$

where $\beta \equiv v$ is the velocity and all variables referring to the through-going particle given in the desired frame of reference (e.g. in the center of mass).

Note that $\partial y / \partial p_{\parallel} = 1/E$. A Lorentz boost β along the direction of the incident particle adds a constant, $\ln(\gamma + \gamma\beta)$, to the rapidity. Rapidity differences, therefore, are invariant to a Lorentz boost. Statistical particle distributions are flat in y for many physics production models. Frequently, the simpler variable *pseudorapidity* η is used instead of rapidity (and sloppy language mixes up the two variables).

The pseudorapidity is a handy variable to approximate the rapidity if the mass and momentum of a particle are not known. It is an angular variable defined by

$$\eta = -\ln \left[\tan \left(\frac{\theta}{2} \right) \right] \quad (72)$$

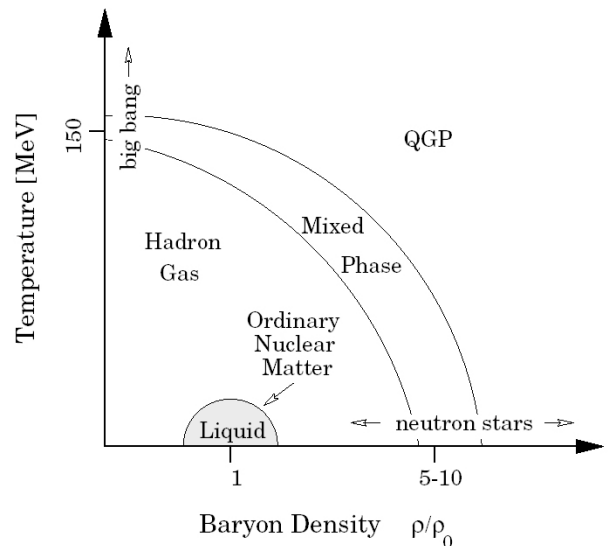


FIG. 15: - As water comes in different phases (solid, liquid, gas), so nuclear matter can come in its normal hadronic form and at sufficiently high temperature and density, in the form of a deconfined state of quarks and gluons. The diagram shows how nuclear matter should behave as a function of density and temperature.

whose inverse function is $\theta = 2 \arctan(e^{-\eta})$, where θ is the angle between the particle being considered and the undeflected beam. η is the same as the rapidity y if one sets $\beta = 1$ (or $m = 0$). Statistical distributions plotted in pseudorapidity rather than rapidity undergo transformations that have to be estimated by using a kinematic model for the interaction.

C. The quark-gluon plasma (QGP)

The primary motivation for studying ultra-relativistic heavy ion collisions is to gain an understanding of the equation of state of nuclear, hadronic and partonic matter, commonly referred to as nuclear matter. Displayed in fig. 15 is a schematic phase diagram of nuclear matter. The behavior of nuclear matter as a function of temperature and density (or pressure), shown in fig. 15, is governed by its equation of state.

Conventional nuclear physics is concerned primarily with the lower left portion of the diagram at low temperatures and near normal nuclear matter density. Here normal nuclei exist and at low excitation a liquid-gas phase transition is expected to occur. This is the focus of experimental studies using low energy heavy ions. At somewhat higher excitation, nucleons are excited into baryonic resonance states, along with accompanying particle production and hadronic resonance formation. In relativistic heavy ion collisions, such excitation is expected to create hadronic resonance matter.

We now briefly discuss the QGP signatures in nucleus-

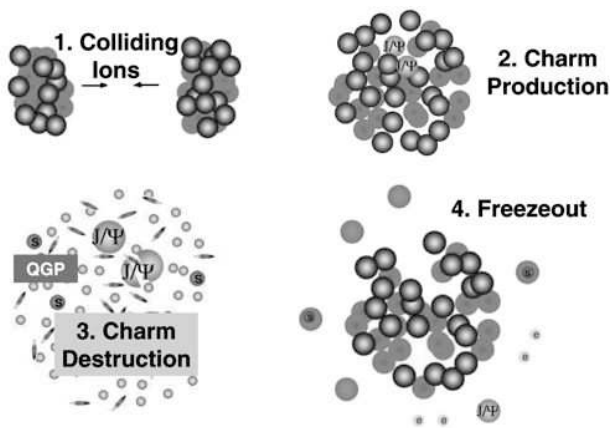


FIG. 16: - Formation and evolution of J/Ψ particles in relativistic heavy ion collisions. After the formation, the J/Ψ s are dissociated in the plasma due to color screening. The end effect is a smaller number J/Ψ s of than expected from pure hadron-hadron multiple collisions.

nucleus collisions. For more details see, e.g., ref. [28, 29]. One group of such signatures can be classified as *thermodynamic variables*. This class involves determination of the energy density ϵ , pressure P , and entropy density s of the interacting system as a function of the temperature T and the baryochemical potential μ_B . Experimental observables can be identified with these variables and thus their relative behavior can be determined. If a phase transition to QGP occurs, a rapid rise in the effective number of degrees of freedom, expressed by ϵ/T^4 or s/T^3 , should be observed over a small range of T . The variables T , s , and ϵ , can be identified with the average transverse momentum $\langle p_T \rangle$, the hadron rapidity density dN/dy , and the transverse energy density dE_T/dy , respectively. The transverse energy produced in the interaction is $E_T = \sum_i E_i \sin \theta_i$, where E_i and θ_i are the kinetic energies of the ejectiles and the emission angles.

Electromagnetic (EM) probes, such as photons and leptons, provide information on the various stages of the interaction without modification by final state interactions. These probes may provide a measure of the thermal radiation from a QGP, if a region of photon energy, or equivalently lepton pair invariant mass, can be isolated for emission from a QGP relative to other processes. However, the yields for EM probes are small relative to background processes, which are primarily EM decays of hadrons and resonances. Lepton pairs from the QGP are expected to be identifiable in the 1-10 GeV invariant mass range. The widths and positions of the ρ , ω , and ϕ peaks in the lepton pair invariant mass spectrum are expected to be sensitive to medium-induced changes of the hadronic mass spectrum

The production of J/Ψ particles in a quark-gluon plasma is predicted to be suppressed (see fig. 16). This is a result of the *Debye screening* of a $c\bar{c}$ pair, initially

formed in the QGP by fusion of two incident gluons. Less tightly bound excited states of the $c\bar{c}$ system, such as Ψ' and χ_c , are more easily dissociated and will be suppressed even more than the J/Ψ .

A long-standing prediction for a signature of QGP formation is the enhancement of strange hadrons. The production of strange hadrons relative to nonstrange hadrons is suppressed in hadronic reactions. This suppression increases with increasing strangeness content of the hadron. In a QGP the strange quark content is rapidly saturated by $s\bar{s}$ pair production in gluon-gluon reactions, resulting in an enhancement in the production of strange hadrons. Thus, multi-strange baryons and strange antibaryons are predicted to be strongly enhanced when a QGP is formed.

The connection between energy loss of a quark and the color-dielectric polarizability of the medium can be established in analogy with the theory of electromagnetic energy loss. Although radiation is a very efficient energy loss mechanism for relativistic particles, it is strongly suppressed in a dense medium by the *Landau-Pomeranchuk effect* [28]. Adding the two contributions, the stopping power of a quark-gluon plasma is predicted to be higher than that of hadronic matter. A quark or *gluon jet* propagating through a dense medium will not only lose energy but will also be deflected. This effect destroys the coplanarity of the two jets from a hard parton-parton scattering with the incident beam axis. The angular deflection of the jets also results in an azimuthal asymmetry. The presence of a quark-gluon plasma is also predicted to attenuate the emission of jet pairs opposite to the trigger jet.

All of the above quark-gluon plasma signatures have been studied to maturity at the CERN (European Organization for Nuclear Research) - SPS (Super Proton Synchrotron) and the BNL (Brookhaven National Laboratory) - RHIC (Relativistic Heavy Ion Collider) facilities. For more details, the following references discuss: (a) direct photons [30, 31], (b) dileptons [32], (c) J/Ψ production [33] and (d) quark in-medium attenuation, also known as high- p_T quenching or jet attenuation [34].

VIII. NUCLEAR REACTIONS IN STARS

A. Hydrogen and CNO cycles

Energy production in stars is a well known process. The initial energy which ignites the process arises from the gravitational contraction of a mass of gas. The contraction increases the pressure, temperature, and density, at the center of the star until values able to start the thermonuclear reactions, initiating the star lifetime. The energy liberated in these reactions yield a pressure in the plasma, which opposes compression due to gravitation. Thus, an equilibrium is reached for the energy which is produced, the energy which is liberated by radiation, the temperature, and the pressure.

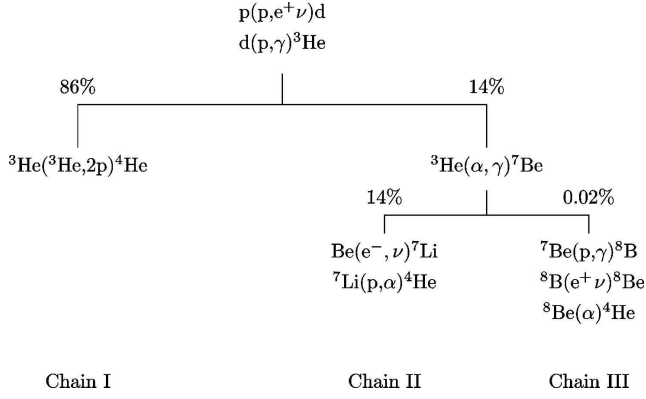
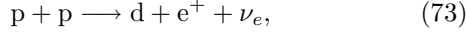


FIG. 17: The p-p chain reaction (p-p cycle). The percentage for the several branches are calculated in the center of the Sun [35].

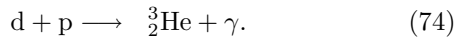
The Sun is a star in its initial phase of evolution. The temperature in its surface is 6000°C , while in its interior the temperature reaches $1.5 \times 10^7\text{K}$, with a pressure given by $6 \times 10^{11}\text{atm}$ and density 150g/cm^3 . The present mass of the Sun is $M_\odot = 2 \times 10^{33}\text{g}$ and its main composition is hydrogen (70%), helium (29%) and less than 1% of more heavy elements, like carbon, oxygen, etc.

What are the nuclear processes which originate the huge thermonuclear energy of the Sun, and that has last 4.6×10^9 years (the assumed age of the Sun)? It cannot be the simple fusion of two protons, or of α -particles, or even the fusion of protons with α -particles, since neither ${}^2_2\text{He}$, ${}^4_4\text{Be}$, or ${}^6_3\text{Li}$, are stable. The only possibility is the proton-proton fusion in the form



which occurs via β -decay, i.e., due to the weak-interaction. The cross section for this reaction for protons of energy around 1 MeV is very small, of the order of 10^{-23}b . The average lifetime of protons in the Sun due to the transformation to deuterons by means of eq. (73) is about 10^{10}y . This explains why the energy radiated from the Sun is approximately constant in time, and not an explosive process.

The deuteron produced in the above reaction is consumed almost immediately in the process



The resulting ${}^3_2\text{He}$ reacts by means of



which produces the stable nucleus ${}^4_2\text{He}$ with a great energy gain, or by means of the reaction



In the second case, a chain reaction follows as

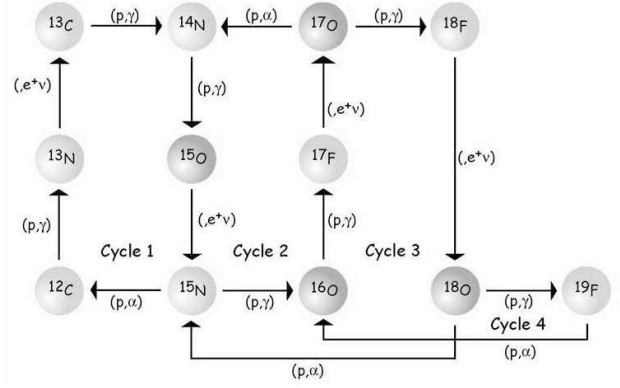
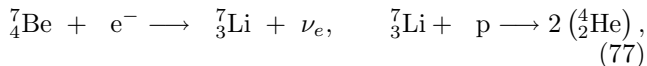
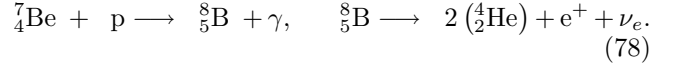


FIG. 18: The CNO cycle. (courtesy of Frank Timmes).

or

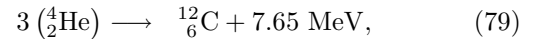


The chain reaction (73)-(78) is called the *hydrogen cycle*. The result of this cycle is the transformation of four protons into an α -particle, with an energy gain of 26.7 MeV, about 20% of which are carried away by the neutrinos (see fig. 17).

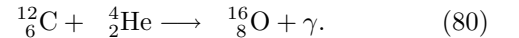
If the star contains heavier elements, another cycle can occur; the *carbon cycle*, or *CNO cycle* [37]. In this cycle the carbon, oxygen, and nitrogen nuclei are catalyzers of nuclear processes, with the end product also in the form $4p \rightarrow {}^4_2\text{He}$. fig. 18 describes the CNO cycle. Due to the larger Coulomb repulsion between the carbon nuclei, it occurs at higher temperatures (larger relative energy between the participant nuclei), up to $1.4 \times 10^7\text{K}$. In the Sun the hydrogen cycle prevails. But, in stars with larger temperatures the CNO cycle is more effective.

After the protons are transformed into helium at the center of a star like our Sun, the fusion reactions start to consume protons at the surface of the star. At this stage the star starts to become a *red giant*. The energy generated by fusion increases the temperature and expands the surface of the star. The star luminosity increases. The red giant contracts again after the hydrogen fuel is burned.

Other thermonuclear processes start. The first is the helium burning when the temperature reaches 10^8K and the density becomes 10^6g.cm^{-3} . Helium burning starts with the triple capture reaction



followed by the formation of oxygen via the reaction



For a star with the Sun mass, helium burning occurs in about 10^7y . For a much heavier star the temperature can reach 10^9K . The compression process followed by the

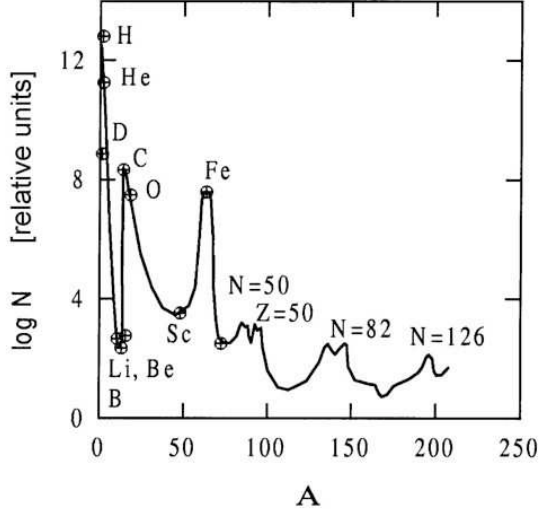


FIG. 19: Relative distribution of elements in our galaxy.

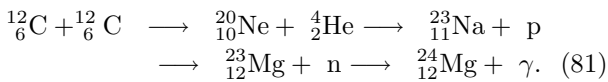
burning of heavier elements can lead to the formation of iron and nickel. After that the thermonuclear reactions are no more energetic and the star stops producing nuclear energy.

B. Synthesis of heavier elements

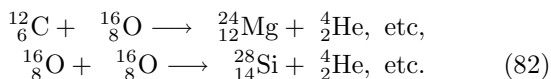
In figure 19 we show the relative distribution of elements in our galaxy. It has two distinct regions: in the region $A < 100$ it decreases with A approximately like an exponential, whereas for $A > 100$ it is approximately constant, except for the peaks in the region of the magic numbers $Z = 50$ and $N = 50, 82, 126$.

The thermonuclear processes (73)-(80) can explain the relative abundance of ${}^4_2\text{He}$, ${}^{12}_6\text{C}$ and ${}^{16}_8\text{O}$. The processes occurring after ${}^4_2\text{He}$ burning mainly form isotopes of ${}^{20}_{10}\text{Ne}$, ${}^{24}_{12}\text{Mg}$ and ${}^{28}_{14}\text{Si}$. We can understand the small abundance of the elements Li, Be and B as due to the small velocity with which they are formed via the reaction (76) and the first equation of (77), while they are rapidly consumed by the second reaction in (77) and the first reaction in (78).

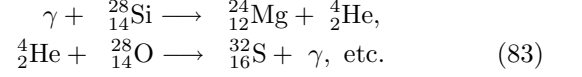
The synthesis of elements heavier than oxygen occur when, after helium burning, a new compression and heating of the star rises the temperature to values higher than 6×10^8 K. This situation ignites an intense carbon burning:



Carbon and oxygen can also burn simultaneously:



For temperatures above 3×10^9 K more photo-nuclear processes appear. These yield more nuclei to be burned and heavier nuclei are produced:



Due to the large number of free neutrons, many (n, γ) -reactions (radiative neutron capture) elements in the mass range $A = 28, \dots, 57$ are formed. This leads to a large abundance of elements in the iron mass region, which have the largest binding energy per nucleon. For elements heavier than iron the nuclear fusion processes do not generate energy.

For $A > 100$ the distribution of nuclei cannot be explained in terms of fusion reactions with charged particles. They are formed by the successive capture of slow neutrons and of β^- -decay. The maxima of the element distribution in $N = 50, 82, 126$ are due to the small capture cross sections corresponding to the magic numbers. This yields a trash of isotopes at the observed element distribution.

C. Thermonuclear cross sections

The nuclear cross section for a reaction between target j and projectile k is defined by

$$\sigma = \frac{\text{number of reactions target}^{-1}\text{sec}^{-1}}{\text{flux of incoming projectiles}} = \frac{r/n_j}{n_k v}. \quad (84)$$

where the target number density is given by n_j , the projectile number density is given by n_k , and v is the relative velocity between target and projectile nuclei. Then r , the number of reactions per cm^3 and sec, can be expressed as $r = \sigma v n_j n_k$, or, more generally,

$$r_{j,k} = \int \sigma |v_j - v_k| d^3 n_j d^3 n_k. \quad (85)$$

The evaluation of this integral depends on the type of particles and distributions which are involved. For nuclei j and k in an astrophysical plasma, obeying a Maxwell-Boltzmann distribution (MB),

$$d^3 n_j = n_j \left(\frac{m_j}{2\pi kT} \right)^{3/2} \exp\left(-\frac{m_j v_j^2}{2kT}\right) d^3 v_j, \quad (86)$$

eq. (85) simplifies to $r_{j,k} = \langle \sigma v \rangle n_j n_k$, where $\langle \sigma v \rangle$ is the average of σv over the temperature distribution in (86).

In astrophysical plasmas with high densities and/or low temperatures, effects of electron screening become highly important. This means that the reacting nuclei, due to the background of electrons and nuclei, feel a different Coulomb repulsion than in the case of bare nuclei. Under most conditions (with non-vanishing temperatures) the generalized reaction rate integral can be

separated into the traditional expression without screening and a screening factor

$$\langle \sigma v \rangle_{j,k}^* = f_{scr}(Z_j, Z_k, \rho, T, Y_i) \langle \sigma v \rangle_{j,k}. \quad (87)$$

This screening factor is dependent on the charge of the involved particles, the density, temperature, and the composition of the plasma. Here Y_i denotes the abundance of nucleus i defined by $Y_i = n_i/(\rho N_A)$, where n_i is the number density of nuclei per unit volume and N_A Avogadro's number. At high densities and low temperatures screening factors can enhance reactions by many orders of magnitude and lead to pycnonuclear ignition.

When in eq. (85) particle k is a photon, the relative velocity is always c and quantities in the integral are not dependent on d^3n_j . Thus it simplifies to $r_j = \lambda_{j,\gamma} n_j$ and $\lambda_{j,\gamma}$ results from an integration of the photodisintegration cross section over a Planck distribution for photons of temperature T

$$r_j = \frac{1}{\pi^2 (c\hbar)^3} \int d^3n_j \int_0^\infty \frac{c\sigma(E_\gamma) E_\gamma^2}{\exp(E_\gamma/kT) - 1} dE_\gamma. \quad (88)$$

There is, however, no direct need to evaluate photodisintegration cross sections, because, due to detailed balance, they can be expressed by the capture cross sections for the inverse reaction $l + m \rightarrow j + \gamma$.

A procedure similar to eq. (88) is used for electron captures by nuclei. Because the electron is about 2000 times less massive than a nucleon, the velocity of the nucleus j is negligible in the center of mass system in comparison to the electron velocity ($|v_j - v_e| \approx |v_e|$). The electron capture cross section has to be integrated over a Boltzmann, partially degenerate, or Fermi distribution of electrons, depending on the astrophysical conditions. The electron capture rates are a function of T and $n_e = Y_e \rho N_A$, the electron number density [36]. In a neutral, completely ionized plasma, the electron abundance is equal to the total proton abundance in nuclei $Y_e = \sum_i Z_i Y_i$ and $r_j = \lambda_{j,e}(T, \rho Y_e) n_j$.

This treatment can be generalized for the capture of positrons, which are in a thermal equilibrium with photons, electrons, and nuclei. At high densities ($\rho > 10^{12} \text{ g.cm}^{-3}$) the size of the neutrino scattering cross section on nuclei and electrons ensures that enough scattering events occur to thermalize a neutrino distribution. Then also the inverse process to electron capture (neutrino capture) can occur and the neutrino capture rate can be expressed similarly to Eq. (88), integrating over the neutrino distribution. Also inelastic neutrino scattering on nuclei can be expressed in this form. Finally, for normal decays, like beta or alpha decays with half-life $\tau_{1/2}$, we obtain an equation similar to Eq. (88) or r_j of the last paragraph with a decay constant $\lambda_j = \ln 2/\tau_{1/2}$ and $r_j = \lambda_j n_j$.

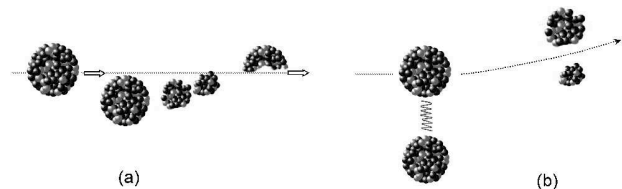


FIG. 20: (a) Schematic description of a nuclear fragmentation reaction producing rare isotopes. The lower fragments are called participants, while the upper one is called the spectator. Using uranium projectiles ($N/Z \sim 1.6$) one expects to produce (light) spectator nuclei of about the same N/Z ratio. (b) Coulomb fission of relativistic projectiles leading to the production of rare isotopes. For a heavy unstable projectile an exchanged photon with the target can give it enough energy to fragment into several types of isotopes.

IX. REACTIONS WITH RADIOACTIVE NUCLEAR BEAMS

The basic research activity in nuclear physics, driven by the desire to understand the forces which dictate the properties of nuclei, has spawned a large number of beneficial applications. Amongst its many progeny we can count reactor- and spallation-based neutron sources, synchrotron radiation sources, particle physics, materials modification by implantation, carbon dating and much more. It is an excellent example of the return to society of investment in basic research.

All of these achievements have been realized by accelerating the 283 stable or long-lived nuclear species we find here on Earth. In recent years, however, it has become evident that it is now technically possible to create and accelerate unstable nuclei and, and there are some 6-7,000 distinct nuclear species which live long enough to be candidates for acceleration. They are the nuclei within the so-called *drip-lines*, the point where the nucleus can no longer hold another particle. This has led to many new opportunities in industry, medicine, material studies and the environment.

Assume that a highly energetic uranium projectile ($N/Z \sim 1.6$) hits a target nucleus in an almost central collision, as shown in fig. 20. A part of the projectile (*participant*) is scrapped off and forms a highly excited mixture of nucleons with a part of the target. A piece of the projectile (*spectator*) flies away with nearly the same velocity of the beam. The neutron-to-proton ratio of the spectator is nearly equal to that of the projectile. Since the N/Z - ratio of light nuclei (stable) is close to one, the fragment is far from the stability line. Statistically, a large number of fragments with different N/Z - ratios is created and several new exotic nuclei have been discovered in this way. These nuclei can be collected in a secondary beam, further accelerated and induce reactions with a target nucleus. This method has become an important tool to study the properties of short-lived isotopes.

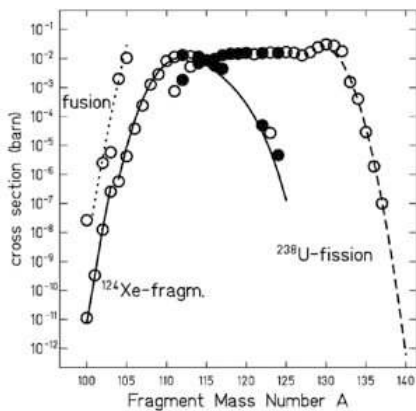


FIG. 21: Production cross sections for the tin isotopes from complete fusion (dotted line), fragmentation (solid line), and projectile fission of ^{238}U (dashed line). The symbols represent experimental data. The fragmentation cross-sections (solid line) have been calculated with a semi-empirical code [Sue00].

Experiments with secondary-beams are limited by reaction cross section and *luminosity*. The luminosity L is defined as the product of beam intensity i and target thickness t , $L = i \cdot t$. The reaction rate N is the product of luminosity and reaction cross section σ_r , $N = \sigma_r \cdot L$. In most of the reactions the usable target thickness is limited by the width of the excitation function (i.e. the cross section as a function of the excitation energy). Production reactions with a wide excitation function covering a broad energy range can profit in luminosity by the use of thick targets.

The condition for fragmentation of heavy ions is that the projectile should move faster than nucleons move inside the nucleus. The projectile energy should be sufficiently above the Fermi domain, e.g. above 100 A MeV. The usable target thickness for these high energies is of the order of several grams per square centimeter, corresponding to 10^{23} atoms/cm². The excitation function for complete fusion of heavy ions, however, has a width of only 10 MeV. This corresponds to a usable target thickness of the order of one milligram per square centimeter or 10^{18} atoms/cm². Consequently beam intensities for the investigation of complete fusion reactions must be by four to five orders higher to achieve the same luminosity as for fragmentation.

Fig. 21 shows as an example the production cross sections for the tin isotopes from complete fusion (dotted line), nuclear fragmentation (solid line), and Coulomb fission of ^{238}U (dashed line). The symbols represent experimental data. The fragmentation cross-sections (solid line) have been calculated with a semi-empirical code [Sue00].

The first experiments with unstable nuclear beams were designed to measure the nuclear sizes, namely the matter distribution of protons and neutrons. For stable nuclei such experiments are best accomplished with elec-

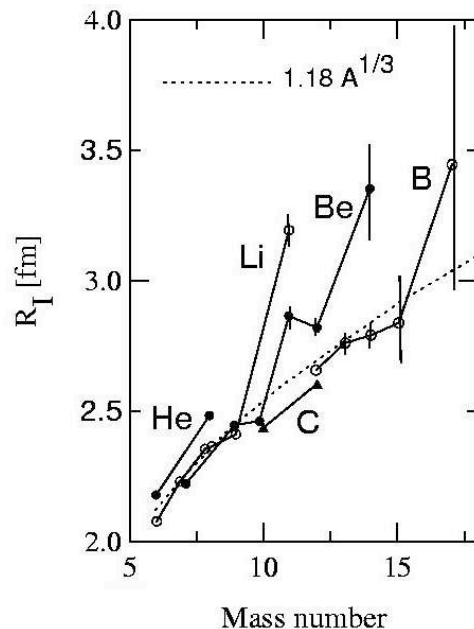


FIG. 22: The matter density radii of several light nuclei compared to the trend $R \sim 1.18 A^{1/3}$ fm (dashed line) for normal nuclei. The solid lines are guides to the eyes.

tron beams, which probe the nuclear charge (proton) distribution. Electron scattering experiments with unstable beams can only be performed in an electron-nucleus collider. But the easiest solution is to measure the *reaction cross section* in collisions of unstable beams with a fixed target nucleus [38].

The reaction cross section in high energy collisions is given by

$$\sigma_R = 2\pi \int [1 - T(b)] b db, \quad (89)$$

where

$$T(b) = \exp \left\{ -\sigma_{NN} \int_{-\infty}^{\infty} dz \int \rho_P(\mathbf{r}) \rho_T(\mathbf{R} + \mathbf{r}) d^3r \right\} \quad (90)$$

with $\mathbf{R} = (\mathbf{b}, z)$. σ_{NN} is the nucleon-nucleon cross section at the corresponding bombarding energy, and $\rho_{P(T)}$ is the projectile (target) matter density distribution. $T(b)$ is known as the *transparency function*. It is the probability that a reaction occurs for a collision with impact parameter b . The exponent $[\sigma_{NN} \int \rho_P(\mathbf{r}) \rho_T(\mathbf{R} + \mathbf{r}) d^3r]^{-1}$ is interpreted as the mean-free path for a nucleon-nucleon collision. The reaction cross sections can be calculated using the matter distributions of the target in eq. 16.

Experimentally it was observed a great increase in the rms radii for the neutron-rich isotopes ^6He , ^8He and ^{11}Li (see figure 22). Thus, the addition of the neutrons to ^4He and ^9Li nuclei increase their radii considerably. This can be understood in terms of the binding energy of the outer

nucleons. The large matter radii of these nuclei have lead the experimentalists to call them “*halo nuclei*”. The binding energy of the last two neutrons in ^{11}Li is about 300 keV. In ^6He it is 0.97 MeV. These are very small values and should be compared with $S_n = 6 - 8$ MeV which is the average binding of nucleons in stable nuclei. Abnormally large radii were also found for other light neutron-rich nuclei.

The matter density radii of these nuclei do not follow the observed trend $R \sim 1.18 A^{1/3}$ fm of normal nuclei. Thus the halo seems to be a common feature of loosely-bound neutron-rich nuclei.

Several other methods have been devised to probe the structure of nuclei far from the valley of stability. Among these are (a) Coulomb dissociation [39], (b) Trojan horse method [40], (c) asymptotic normalization coefficients [41], (d) heavy ion charge-exchange [42], (e) knockout [43] and (f) fusion reactions [44]. These methods yield different insights into the structure of exotic nuclei and comprise most of experiments in radioactive beam facilities [45].

Reactions producing rare nuclear isotopes has opened a new research front in nuclear physics with applications

in many areas of science: (a) the rapid production of short-lived nuclei, many of which are poorly known, is important for astrophysics (r-process) and cosmology, (b) nuclear medicine benefits from studies of new nuclear isotopes, (c) and the list goes on. But the basic question still remains: what combinations of neutrons and protons can make up a nucleus? The experimental detection of new nuclear isotopes is an ongoing research which will ultimately lead to new insight and development of nuclear science, with enormous profit for mankind [46].

Acknowledgments

The author is grateful to Prof. Reinhard Stock and Prof. Konrad Gelbke for their support and encouragement. This work was supported in part by funds provided by the U.S. Department of Energy (DOE) under contract No. DE-FG02-08ER41533 and DE-FC02-07ER41457 (UNEDF, SciDAC-2), and the Research Corporation under Award No. 10497.

-
- [1] C.A. Bertulani, “Nuclear Reactions”, Wiley Encyclopedia of Physics, Wiley-VCH, Berlin, 2009.
- [2] E. Rutherford, *Phil. Mag.* **21**, 669 (1911).
- [3] B. W. Ridley and J. F. Turner, *Nucl. Phys.* **58**, 497 (1964).
- [4] N. Bohr, *Nature*, **137**, 344 (1936).
- [5] S. N. Ghoshal, *Phys. Rev.* **80**, 939 (1950).
- [6] A. Tsveter, *Nucl. Phys.* **A185**, 433 (1972).
- [7] H. Marshak, A. Langsford, C. Y. Wong and T. Tamura, *Phys. Rev. Lett.* **20**, 554 (1968).
- [8] K. W. McVoy, *Ann. Phys.* **43**, 91 (1967).
- [9] H. Feshbach, C. E. Porter and V. F. Weisskopf, *Phys. Rev.* **90**, 166 (1953).
- [10] H. Feshbach, *Theoretical Nuclear Physics - Nuclear Reactions* (New York: John Wiley), 1992.
- [11] V.F. Weisskopf and D.H. Ewing, *Phys. Rev.* **54**, 472 (1940).
- [12] W. Hauser and H. Feshbach, *Phys. Rev.* **87**, 366 (1952).
- [13] U. Facchini and E. Saetta-Menichella, *Energ. Nucl.* **15** 54 (1968).
- [14] F. G. Perey, *Phys. Rev.* **131**, 745 (1963).
- [15] K. Miura *et al.*, *Nucl. Phys.* **A467**,79 (1987).
- [16] J. B. Natowitz, *Phys. Rev.* **C1**, 623 (1970).
- [17] L. Kowalsky, J. C. Jodogne and J. M. Miller, *Phys. Rev.* **169**, 894 (1968).
- [18] A. M. Zebelman and J. M. Miller, *Phys. Rev. Lett.* **30**, 27 (1973).
- [19] E. McMillan and P. H. Abelson, *Phys. Rev.* **57**, (1940) 1185.
- [20] Yu. Ts. Oganessian *et al.*, *Phys. Rev.* **C 74**, 044602 (2006).
- [21] A. Leprêtre *et al.*, *Nucl. Phys.* **A219**, 39 (1974).
- [22] P. Axel, *Phys. Rev.* **126**, 671 (1962).
- [23] S. Mordechai *et al.*, *Phys. Rev. Lett.* **61**, 531 (1988).
- [24] C. A. Bertulani and G. Baur, *Phys. Lett.* **B174**, 23 (1986); *Phys. Rep.* 163, 299 (1988).
- [25] R. Schmidt *et al.*, *Phys. Rev. Lett.* **70**, 1767 (1993).
- [26] L. Frankfurt, M. Strikman and C. Weiss, *Ann. Rev. Nucl. Part. Sci.* **55**, 403 (2005).
- [27] P. Danielewicz, *Phys. Rev.* **C51**, 716 (1995).
- [28] C.Y. Wong, *Introduction to high energy heavy ion collisions*, 1994 (Singapore: World Scientific).
- [29] R.C. Hwa and X.N. Wang, eds., *Quark-Gluon Plasma 3*, 2004 (Singapore: World Scientific).
- [30] M.M. Aggarwal *et al.*, *Phys. Rev. Lett.* **85**, 3595 (2000).
- [31] S. Bathe *et al.*, *Nucl. Phys.* **774**, 103 (2006).
- [32] S. Damjanovic *et al.*, *Nucl. Phys.* **A774**, 715 (2006).
- [33] A. Adare *et al.*, *Phys. Rev. Lett.* **98**, 232302 (2007).
- [34] H. Buesching *et al.*, *Nucl. Phys.* **774**, 103 (2006).
- [35] J.N. Bahcall, *Neutrino Astrophysics*, 1989 (Cambridge: Cambridge University Press)
- [36] G.M. Fuller, W.A. Fowler and M. Newman, *Ap. J.* **293**, 1 (1985).
- [37] H. A. Bethe, *Phys. Rev.* **55**, 434 (1939).
- [38] I. Tanihata *et al.*, *Phys. Rev. Lett.* **55**, 2676 (1985).
- [39] G.Baur, C.A.Bertulani and H.Rebel, *Nucl. Phys.* **A458**, 188 (1986).
- [40] G. Baur, *Phys. Lett.* **B178**, 135 (1986).
- [41] H. M. Xu, C. A. Gagliardi, R. E. Tribble, A. M. Mukhamedzhanov, and N. K. Timofeyuk, *Phys. Rev. Lett.* **73**, 2027 (1994).
- [42] M. Steiner *et al.*, *Phys. Rev. Lett.* **76**, 26 (1996).
- [43] P.G. Hansen and J. A. Tostevin, *Annu. Rev. Nucl. Part. Sci.* **53**, 219 (2003).
- [44] L.F. Canto, P. R. S. Gomes, R. Donangelo, and M. S. Hussein, *Phys. Rep.*, **424**, 1 (2006).
- [45] D.F. Geesaman, C.K. Gelbke, B.M. Sherrill, R.V.F. Janssens, *Annu. Rev. Nucl. Part. Sci.*, **56**, 53 (2006).

[46] T. Baumann, et al., *Nature* **449** (2007) 1022.

Further Reading

C.A. Bertulani and P. Danielewicz, *Introduction to Nuclear Reactions*, IOP Publishing, London, 2004.

C.A. Bertulani, *Nuclear Physics in a Nutshell*, Princeton University Press, Princeton, 2007.

Pawel Danielewicz, Roy Lacey and William G. Lynch, *Determination of the Equation of State of Dense Matter*, *Science* **298**, 1592 (2002).

Herman Feshbach, *Theoretical Nuclear Physics, Nuclear Reactions*, Wiley-Interscience, New York, 1993.

P. Fröbrich and R. Lipperheide, *Theory of Nuclear Reactions*, Oxford University Press, Oxford, 1996.

Christian Iliadis, *Nuclear Physics of Stars*, Wiley, New York, (2007).

J.S. Lilley, *Nuclear Physics: Principles and Applications*, Wiley, New York, 2001.

Norman K. Glendenning, *Direct Nuclear Reactions*, World Scientific, Singapore, 2004.

Samuel S. M. Wong, *Nuclear Physics*, Wiley, New York, 2004.

C.Y. Wong, *Introduction to high energy heavy ion collisions*, World Scientific, Singapore, 1994.

This figure "exper.jpg" is available in "jpg" format from:

<http://arxiv.org/ps/0908.3275v1>